Comparing and Quantifying Indoor Performance of Organic Solar Cells

*Dana Lübke, Paula Hartnagel, Johanna Angona and Thomas Kirchartz**

D. Lübke, P. Hartnagel, J. Angona
IEK5-Photovoltaik, Forschungszentrum Jülich, 52425 Jülich, Germany

Prof. T. Kirchartz
IEK5-Photovoltaik, Forschungszentrum Jülich, 52425 Jülich, Germany
Faculty of Engineering and CENIDE, University of Duisburg-Essen, Carl-Benz-Str. 199, 47057 Duisburg, Germany
E-mail: t.kirchartz@fz-juelich.de

Keywords: indoor photovoltaics, comparable efficiencies, non-fullerene acceptors, Shockley-Queisser limit indoors

With increasing efficiencies of non-fullerene acceptor-based organic solar cells, this thin-film technology is becoming a promising candidate for indoor light harvesting applications. However, the lack of standardized comparison methods makes it difficult to quantify progress and to compare indoor performance. Herein, we present a simple method to calculate the efficiency of solar cells under any possible light source and illuminance with only using simple standard measurements (current-voltage curves and quantum efficiency). Thereby, equal evaluation conditions are ensured, so that we can rank and compare indoor solar cells according to their efficiency. Efficiencies are shown to typically vary by ±20 % when using different LED spectra with color temperatures ranging from 2700 to 6500 K. Calculations based on a detailed balance model indicate that the optimal bandgap of the absorber material depends on the used light source and ranges between 1.75 eV and 2 eV. Our approach is validated by comparison with literature data and many calculated efficiencies match well with experimental data obtained with a specific light source. However, some reported efficiencies cannot be reproduced with our model, which highlights the need of reassessing low light measuring techniques. Furthermore, a script is provided for use by the community.

1. Introduction

With the development and application of a broad range of strongly absorbing non-fullerene acceptors in the last five years, the power conversion efficiencies of organic solar cells have increased rapidly and are now approaching 20%.[1–6] While these efficiencies are still lower than those of crystalline Si (silicon) and other inorganic solar cell technologies[7], using organic molecules offers a range of advantages that make those materials attractive for applications other than utility-scale electricity supply. An important application that benefits from the tuneability of band gaps in molecular semiconductors is the use of OPV (organic photovoltaics) for indoor light harvesting . The market of the internet of things (IoT) is emerging remarkably and demands to drive high amounts of off-grid low power consumption devices.[8–13] The possibility to produce solution-based, low-cost and flexible solar foils makes OPV a good candidate to fulfil this demand. Furthermore, the absorption spectra of the active materials can be tuned chemically to match different light sources.

Although efficiencies for iOPV[14–35] (indoor organic photovoltaics) and other emerging iPV (indoor photovoltaics) technologies such as halide perovskites[36–43] or dye-sensitized solar cells[44–50] have improved substantially, it is hard to quantify progress and determine champion solar cells due to a lack of standardized comparison methods.[12,51,52] Different authors use different conditions to evaluate the performance of their devices. The set-ups differ in the illuminance value (ranging typically from 200 lux to 1000 lux) and the source of light, namely light emitting diodes (LED) or fluorescent lamps (FL) with varying emission spectra and color temperatures. This makes it difficult to compare devices and regularly leads to the publication of tables or figures where data is compared for different input spectra and illuminances[43,53,54]. The exact spectrum and intensity are, however, more than just a minor inconvenience for data comparison but can have a major impact on the output power at a given illuminance and the efficiency. This is due to several reasons. First, the presence of shunts[55–57] can have a substantial effect on the dependence of open-circuit voltage and fill factor on the light intensity

under indoor conditions.[55,56,58] Second, the short-circuit current at a given illuminance strongly depends on the overlap of the materials' absorption spectra and the spectral emission power of the light source.[53,59] The exact spectrum is even more critical than for outdoor illumination, because indoor light sources have much more narrow spectra with strong emission between wavelengths of 400 nm and 700 nm[60,61] as compared to the AM1.5G spectrum.

In the worst-case scenario, an otherwise well-performing solar cell could exhibit low efficiencies if the color temperature of the light source is not suitable to the specific absorber bandgap. Standardizing indoor spectra as done for outdoor efficiency measurements is not practical given the substantial spectral differences between the used light sources. Furthermore, the intensity of the emission power determines the input power P_{in}, i.e. the denominator of the efficiency $\eta = P_{out}/P_{in}$, where P_{out} is the output power of the solar cell. Using a lux meter is an easy but highly inaccurate method to test the illuminance[31,59,62] and therefore should not be used to evaluate efficiencies in publications. Absolute measurements of the spectral irradiance would be needed to determine precise input powers.

In the literature, several approaches to either analyze the problem or present solutions to the challenge of comparability have been presented in recent years. Chen et al.[51] presents a large round robin study on dye-sensitized solar cells reporting relative deviations of indoor PCEs among different laboratories of up to 152%. Virtuani et al. simulated performance parameters of a copper-poor Cu(In,Ga)Se_2 cell under different indoor illumination levels and spectral distributions.[52] A very recent study of Cui et al. aims to provide guidance to a more precise way of measuring indoor efficiencies. They identified different measurement errors, which originate from the use of artificial light sources and measurement methods (temporal stability and spatial inhomogeneities of light sources, edge effects, using lux meters) and proposed practical measuring protocols.[59,62] While these studies focus on the conditions and circumstances generated by the use of artificial light sources, a proposed method to quantify and compare (existing) data from different laboratories is currently still missing.

To address the problem of unavoidable arbitrariness of different light sources one needs to find figures of merit (FOMs), which are easy to use by the PV community. In this analysis, we present an evaluation method based on the measurement of the external quantum efficiency ($Q_{\mathrm{e,PV}}$) combined with relative measurements of the spectral irradiance and current-voltage (*JV*) characteristics at different light intensities with one light source. With this combination of relatively simple methods, it is possible to calculate the theoretical efficiency of a solar cell for light sources with different emission spectra and at different light intensities and thus, enable a fair comparison of the indoor performance of different solar cells. Based on this approach, we present a meta-analysis of the current state of the art iOPV and compare this state of the art with thermodynamic efficiency limits under indoor illumination. Although we focus in this study on the application of our method to OPV, the method can be applied to other PV technologies. Furthermore, we provide a script that allows the community to calculate the efficiencies of their own devices given the above input data. Thereby, our approach does not only provide a solution for researchers, who want to compare their data, but also gives a practical perspective to companies and costumers, who want to choose the optimal absorber blend for a given illumination condition or estimate the needed area for a given power demand of an IoT device.

2. Theoretical background

The determination of photovoltaic power conversion efficiencies depends on the spectrum of the used light source as the efficiency scales inversely with the input power. In section 2.1, we give the theoretical background to calculate the input power density at a defined illuminance level with a relative irradiance spectrum. In section 2.2, we demonstrate how to adjust the measured output power of the solar cell to the defined illumination level. Together, section 2.1 (dealing with the input power of the light source) and section 2.2 (dealing with the output power of the solar cell) are describing our proposed method, which enables a calculation of the efficiency under any light source spectrum and illuminance intensity with only using standard measuring methods ($Q_{\mathrm{e,PV}}$, *JV* and spectrometer). A stepwise instruction how to use this method

and a link to the *Matlab* code can be found in the method section and additionally, **Figure 1** gives an overview on how to use our method. As this method is calculation based, it gives not only the freedom to compare literature data, but also serves the practical purpose to scan for the best absorber material for a given illumination.

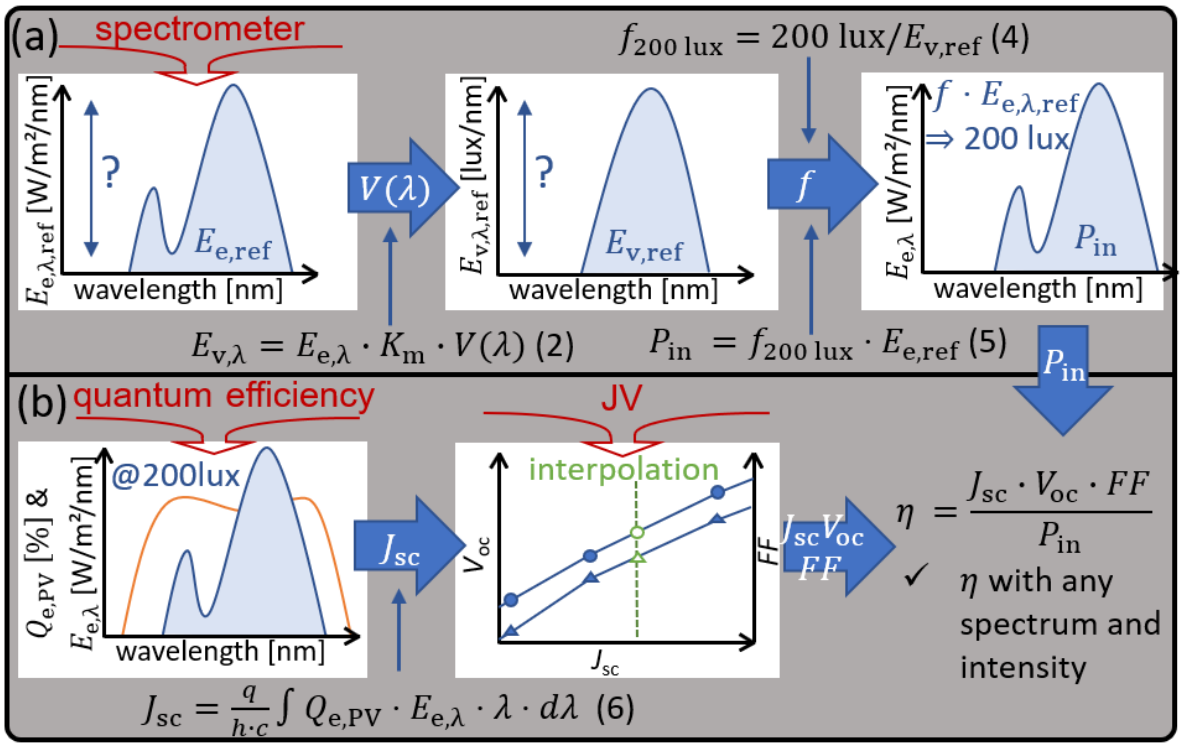

Figure 1. Overview to our proposed method, including measurements (red) and calculations (arrows). Details on the normalization of reference spectra to calculate the input power (a) are described in section 2.1 and the determination of the input power (b) is discussed in section 2.2..

2.1 Determination of input power densities at constant illuminance

The efficiency $\eta = P_{\mathrm{out}}/P_{\mathrm{in}}$ is determined by the ratio of the output power P_{out} of the solar cell and the input power P_{in} from the light source. The integration of the spectral irradiance $E_{\mathrm{e},\lambda}$ (for indoor applications usually in µW/cm²/nm) over the wavelength λ results in the power density or irradiance

$$P_{\mathrm{in}} = E_{\mathrm{e}} = \int E_{\mathrm{e},\lambda} \cdot \, d\lambda \tag{1}$$

of the light source given typically in µW/cm². For indoor light applications, photovoltaic performance is usually quantified at a given illuminance, which is a quantity that takes the sensitivity of the human eye into account. Thus, the idea is to compare at an equal brightness perceived by the human observer rather than at a standardized power density as is done for outdoor performance measurements. To determine the illuminance from the power density, we first have to multiply the spectral irradiance $E_{\mathrm{e},\lambda}$ with the standard sensitivity curve of the human eye $V(\lambda)$ and the coefficient $K_{\mathrm{m}} = 683\ \mathrm{lm/W}$ to arrive at

$$E_{\mathrm{v},\lambda} = E_{\mathrm{e},\lambda} \cdot K_{\mathrm{m}} \cdot V(\lambda). \tag{2}$$

Here, $E_{\mathrm{v},\lambda}$ is the spectral illuminance in lux/nm, which then can be integrated as in Equation 1 to obtain the illuminance E_{v} in lux. As stated in Ref. [38] the most accurate way to determine the illuminance is to measure the absolute spectral irradiance and then calculate the illuminance. Unfortunately, most publications lack in absolute data and only provide the relative spectral irradiance of their LED[14,15,17,21,25,26,33,63], which is much easier to obtain, in some cases not even relative light source spectra are given.[24,34,64] Hence, in many publications the illuminance is determined by a lux meter[15,16,21,25,29,30,32] and then the input power density is calculated with the measured illuminance and the relative spectra of the light source. The lux meter, however, only really measures relative photon densities and converts those to irradiance values using an assumption about the spectral shape of the light source. Typically, the assumption used is the so-called CIE standard illuminant A, i.e. a black body with a temperature of 2856 K[65] which

is similar to the spectrum of an incandescent light bulb but not to the spectrum of an LED.[66] While lux meters offer the option to use correction factors to account for different spectra of light sources, it is advisable to not rely entirely on a lux meter for the determination of illuminances and the correct calculation of an efficiency.[31,51,59,62,67]

Fortunately, if we want to know the spectral irradiance of an LED at a given illuminance (e.g. 200 lux), we can just calculate it, even if we only have the relative spectral irradiance at an arbitrary intensity. We know that e.g.

$$E_{\mathrm{v},200\ \mathrm{lux}} := 200\ \mathrm{lux} \coloneqq \int E_{\mathrm{v},\lambda,200\ \mathrm{lux}}\, d\lambda = f_{200\ \mathrm{lux}} \cdot \int E_{\mathrm{v},\lambda,\mathrm{ref}}\, d\lambda. \quad (3)$$

where $f_{200\ \mathrm{lux}}$ is a factor that we have to multiply a known reference spectrum $E_{\mathrm{v},\lambda,\mathrm{ref}}$ with to obtain the spectral illuminance $E_{\mathrm{v},\lambda,200\ \mathrm{lux}} = f_{200\ \mathrm{lux}} E_{\mathrm{v},\lambda,\mathrm{ref}}$ at 200 lux. In Equation 3, we know all terms except $f_{200\ \mathrm{lux}}$ which we can therefore determine as

$$f_{200\ \mathrm{lux}} = 200\ \mathrm{lux} / \int E_{\mathrm{v},\lambda,\mathrm{ref}}\, d\lambda. \quad (4)$$

Initially, we do not know the integration kernel $E_{\mathrm{v},\lambda,200\ \mathrm{lux}}$ but we do know the result of the integral ($E_{\mathrm{v},200\ \mathrm{lux}} := 200\ \mathrm{lux}$) and we assume that the LED spectrum does not change its shape, when the input power of the LED is changed to give different illuminances. Hence, the desired information, namely $E_{\mathrm{v},\lambda,200\ \mathrm{lux}}$, follows as $f_{200\ \mathrm{lux}} \cdot E_{\mathrm{v},\lambda,\mathrm{ref}}$.

To correctly determine efficiencies, we need to accurately determine the input power density $P_{\mathrm{in}}(@200\ \mathrm{lux})$ (irradiance) which can be calculated with the factor $f_{200\ \mathrm{lux}}$ and the measured relative spectral irradiance $E_{\mathrm{e},\lambda,\mathrm{ref}}$ via

$$P_{\mathrm{in}}(@200\ \mathrm{lux}) = E_{\mathrm{e}}(@200\ \mathrm{lux}) = f_{200\ \mathrm{lux}} \int E_{\mathrm{e},\lambda,\mathrm{ref}}\, d\lambda. \quad (5)$$

Note, that this calculation is exemplarily done for a set illuminance of 200 lux but can be performed for any illuminance, resulting in a set of factors *f* for different illuminances.

2.2 Adjusting the output power and visualization of the method

To illustrate the dependence of the input spectral irradiance $E_{e,\lambda}$ of the used LED on the resulting efficiency, we discuss the effect of two exemplary LED light sources. The LEDs have the same color temperature of 2700 K according to manufacturer information but nevertheless have slightly different spectra. **Figure 2**(a) displays the spectral irradiance $E_{e,\lambda}$ of the light source used in this work and of the light source used by Cui et al. in Refs. [30,31]. Note that the spectral irradiances are already normalized to 200 lux as described above, which can be seen in the integral illuminance in Fig. 1(b) (right y-axis). The LED used in this work exhibits an integral power density of 77.85 µW/cm² and the LED of Cui et al. has a power density of 60.4 µW/cm². Although the LEDs are similar at first sight, the small shift of the LED peak of Cui et al. to lower wavelengths results in considerably different irradiances. The closer the LED peak is to the maximum of $V(\lambda)$ at 555 nm, the more light usable to the human eye is in the spectra. As a consequence, smaller irradiances are needed to reach a certain constant illuminance. Thus, light sources with spectra close to $V(\lambda)$ decrease the input power at constant illuminances.

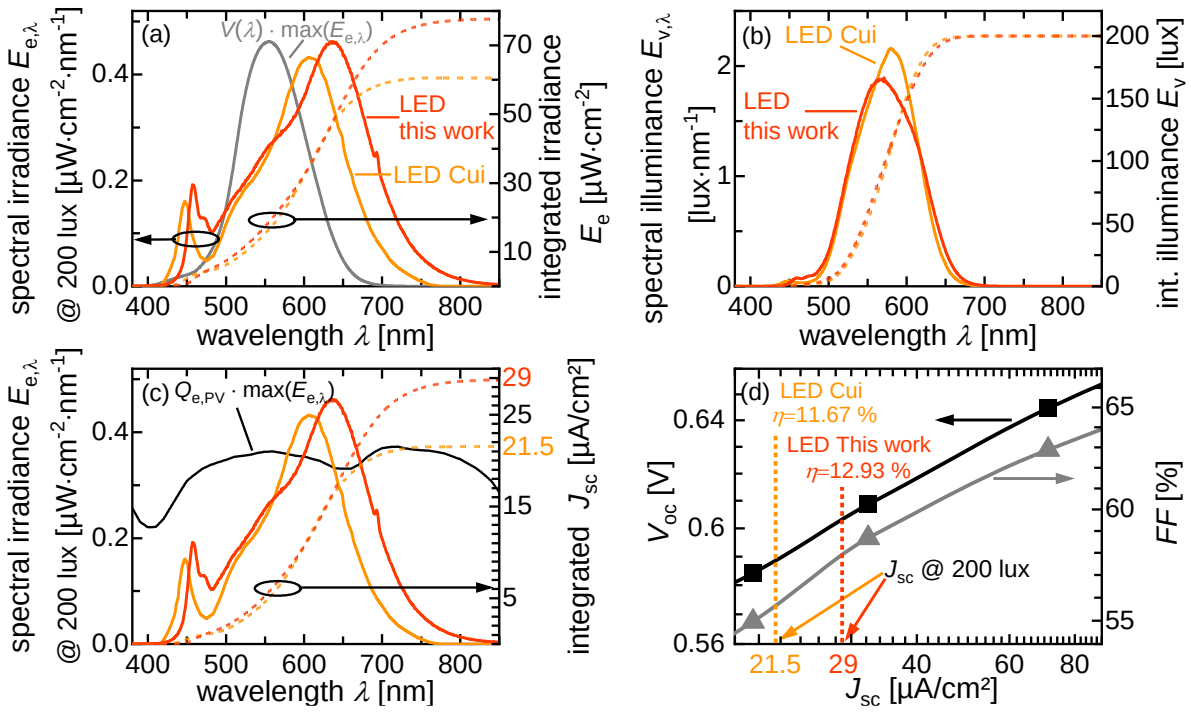

Figure 2. (a) Relative spectral irradiance $E_{e,\lambda}$ of two light sources with 2700 K normalized to 200 lux as described in section 2.1. Orange lines are the LED data used in this work and yellow lines indicate LED data of Ref. [30,31]. The accumulated integral irradiances are depicted as well in dashed lines on the right axis. By multiplication of the spectral irradiance with the luminous efficacy curve $V(\lambda)$ the spectral illuminance in Figure 2(b) is obtained. The integral illuminance (dashed lines) leads to the same value for both spectra due to the normalization of $E_{v,\lambda}$ to 200 lux. In Figure 2(c) the quantum efficiency $Q_{e,PV}$ of a PBDB-TF-T1:Y12 sample is depicted, which is multiplied with the maximum spectral irradiance. The integration of the product of the $Q_{e,PV}$ and the spectral irradiance $E_{e,\lambda}$ gives the short circuit current density, which is shown with dashed lines accumulatively in Figure 2(c) on the right axis (Equation 6). In Figure 2(d) the short circuit current densities are plotted on a double-logarithmic scale versus open-circuit voltages (squares) and fill factors (triangles), which were obtained by *JV* measurements. The lines exhibit interpolated values between the measured points. The output power of the solar cell at the specific illumination of 200 lux can be calculated by the J_{sc}, determined in Fig. 1(c) right axis, and the interpolated values of V_{oc} and FF. These interpolated values are emphasized with the yellow and orange dashed lines in panel (d). Finally, the efficiency at 200 lux can be determined from the exact input power and the output power of the solar cell.

The external quantum efficiency ($Q_{e,PV}$) and the spectral irradiance are integrated over the wavelength to calculate the resulting short circuit current density

$$J_{sc} = \frac{q}{h \cdot c} \int Q_{e,PV} \cdot E_{e,\lambda} \cdot \lambda \cdot d\lambda, \quad (6)$$

Here q is the elementary charge, h is Planck's constant and c the speed of light. Equation 6 assumes that J_{sc} is linear with light intensity at the low light intensities relevant for indoor illumination and the similarly low light intensities that are typically present in a quantum efficiency measurement. If this condition of linearity is fulfilled, Equation 6 should provide a precise value for J_{sc} under the spectral irradiance $E_{e,\lambda}$. When applying the proposed method to other solar cell technologies, care has to be taken that Equation 6 is still valid. In perovskite[68] as well as dye-sensitized solar cells[69], deviations between the J_{sc} determined from Equation 6 and from solar simulator measurements have been reported in some cases. In organic solar cells,

deviations between J_{sc} from Equation 6 and from solar simulator data have also been reported.[70] However, this typically only affects J_{sc} values measured at intensities around one sun and higher while there should be no non-linearities at the low light intensities relevant for indoor applications.[71,72]

Figure 2(c), the quantum efficiency normalized to the maximal spectral irradiance and the resulting integrated short circuit current densities are shown for an organic solar cell with PBDB-TF-T1:BTP-4F-12 (PBDB-TF-T1:Y12) as the absorber material fabricated in our group, which was first shown in Ref. [73]. The onset of the $Q_{\mathrm{e,PV}}$ is 872 nm and photovoltaic parameters at 1 sun illumination can be found in the supplementary information. With the LED of Cui and co-workers a short circuit current density J_{sc} of 21.5 µA/cm² is obtained. With the slightly broader spectrum and the higher input power of the LED in our work, a higher short circuit current density of 28.8 µA/cm² is reached. To determine the output power $P_{\mathrm{out}} = J_{\mathrm{sc}} V_{\mathrm{oc}} FF$ of the solar cell, current-density-voltage characteristics at different light intensities close to the lux levels of interest are measured. The $V_{\mathrm{oc}}(J_{\mathrm{sc}})$ and the $FF(J_{\mathrm{sc}})$ pairs are displayed in Figure 2(d) on a double logarithmic scale. By a pchip-interpolation (piecewise cubic hermite interpolating polynomial, see comment in the method section) of $V_{\mathrm{oc}}(J_{\mathrm{sc}})$ and $FF(J_{\mathrm{sc}})$ to the calculated J_{sc}, P_{out} can be calculated for any given relative light source spectrum or illumination intensity. We assume that the open-circuit voltage and the fill factor are only dependent on the short circuit current density and not on the spectrum of the light source. With increasing photon energy, photons excite charge carriers to higher energy levels, which lose the excess energy by thermalization which eventually leads to the same V_{oc}. Measurements in Refs. [31–33] (Table S7 in Ref. [32] and Table 2 in Ref. [31] and Table S1/Table S2 in Ref. [33]) suggest that this assumption holds true and additional measurements can be found in Figure S1 in the supplementary information.

As the J_{sc} increases for the LED in this work compared to the one for the LED of Cui and co-workers, the V_{oc} and the FF also shift to higher values. Consequently, the output power increases from 7.0 µW/cm² to 10.1 µW/cm² for the LED of Cui et al. and the LED used in our work, respectively. Although the peak closer to 555 nm of the LED of Cui et al. boosts the efficiency with a lower input power as stated above, the efficiency is 11.67 % compared to the LED of our work with 12.93 %. For the LED of our work the gain of J_{sc} and therefore P_{out} due to the higher input power outweighs the efficiency loss due to the higher input power in the denominator, resulting in an absolute efficiency increase of 1.26 %. The method presented above enables an in-depth analysis of the efficiency of organic solar cells under different light conditions. This example shows that apparently small differences in the spectral irradiance can have considerable effects on the resulting efficiency. Firstly, a good overlap of the spectral irradiance and the luminous efficacy curve increases the efficiency at a given illuminance (i.e. 200 lux) due to lower input powers. Nevertheless, these lower input powers decrease the output power of the solar cell. Secondly, a maximized overlap of the samples' quantum efficiency and the spectral irradiances ensures a high J_{sc} and therefore a high output power. The interplay of these two effects can hardly be seen at first sight and makes the proposed analysis very valuable to find best performing combinations of light sources and absorber materials.

3. Results

3.1 Verification of method

To verify the method presented above, we apply the calculation to data of Cui and co-workers as they measured the spectral irradiance in absolute quantities with a calibrated spectrometer.[30] Cui et al. presented iOPV cells with PBDB-TF as donor and IT-4F, ITCC and $PC_{71}BM$ as acceptor materials under illumination with a white LED with a color temperature of 2700 K.[30] Note that this is a relatively low color temperature for a white LED, i.e. one with more photons in the red and less in the blue spectral region. The results are shown in **Figure 3**

on a double-logarithmic scale. Filled symbols represent the original values of the three samples for illuminances of 200, 500 and 1000 lux as provided in Ref. [30], whereas blank symbols show the results of our calculation. Firstly, we address the normalization of the spectral irradiance to the applied lux levels. The integration according to Equation 1 and Equation 2 gives a $E_{\mathrm{v,ref}}$ of 46425.97 lux which leads to normalization factors of 0.0043, 0.0108 and 0.02154 for the $E_{\mathrm{v,set}}$ of 200, 500 and 1000 lux, respectively. Note that we apply the calculation to relative spectral irradiance data, although absolute measurements are available in order to prove the applicability to relative data. The integration of the factorized reference spectra $f \cdot E_{\mathrm{e},\lambda,\mathrm{ref}}$ results in input power densities of 60.38, 150.96, and 301.91 µW/cm² for 200, 500 and 1000 lux, respectively. The input power densities are shown in Figure 3(a) and match well with the original absolute data. The integration according to Equation 6 gives J_{sc} values, which are in good agreement with the original J_{sc} values of Cui and co-workers as well and are depicted in Figure 3(b). Only the PBDB-TF:PC_{71}BM cell shows a slight deviation with a calculated J_{sc} of 18.63 µA/cm² to the original value of 18.9 µA/cm², which is likely to origin from slight discrepancies in the J_{sc} from the *JV* measurement and the J_{sc} from $Q_{\mathrm{e,PV}}$. As the V_{oc} and FF are computed by interpolation, a well matching J_{sc} automatically results in a good match of the values for V_{oc} and FF, which can be seen in the supplementary information in Figure S2. Figure 3(c) and 3(d) show the resulting output power densities and efficiencies. Apart from a slight deviation of the PBDB-TF:PC_{71}BM sample due to the J_{sc} difference, the calculated output power densities and efficiencies are in excellent agreement with the original data.

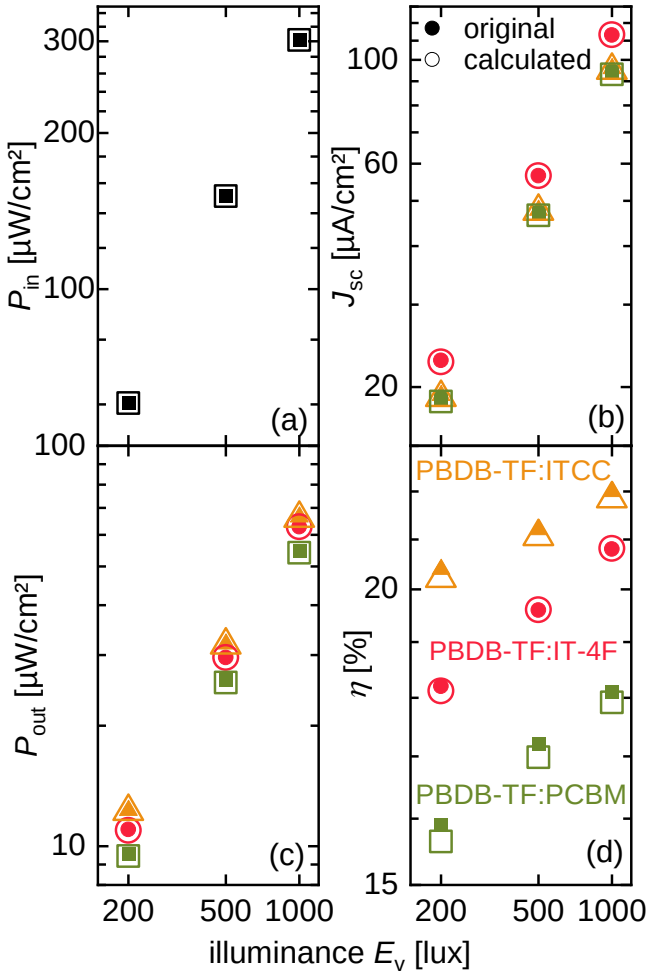

Figure 3. Comparison of original data of Cui et al. from Ref. [30] (filled symbols) and our calculation (blank symbols) on a double-logarithmic scale. Illuminance dependent data of P_{in} (a), J_{sc} (b), P_{out} (c) and the efficiency η (d) are shown. The overlap of filled and blank symbols proves the correctness of the performed calculation.

In the supplementary information a detailed analysis of a range of published data is shown (Figure S3 - Figure S9), where the necessary data was available. In about 65 % of the studied data the efficiency stated in the publication and calculated with our method are in good agreement, meaning only deviating about 1 % (in total). In the other 35 % of the evaluated data the stated and the measured absolute efficiency is deviating >3% in total, in worst cases > 8% in total, which emphasizes the need of establishing low light measuring protocols. The deviations can have the following reasons: Firstly, inconsistencies in the theoretical input powers (calculated with the relative LED spectra normalized to 200 lux) and the given input

powers in the references imply that the illumination is not measured precisely. Therefore, the performance parameters are measured at an arbitrary point of illumination. If the lux meter for instance underestimated the illumination and the measured points would be on a slightly higher illuminance in reality, this error propagates to all performance parameters. Consequently, the J_{sc} of the apparent 200 lux would seem higher, because in reality it might have been measured at say 210 lux. A detailed discussion can be found in the supplementary information. Secondly, as stated in Ref. [59], the theoretical J_{sc} (J_{cal} in the Ref. [59]) should be consistent with the *JV* measurement, which is not the case for many publications. This inconsistency indicates, that either the $Q_{\mathrm{e,PV}}$ or the LED spectra are of insufficient accuracy. Consequently, an overlap of calculated data points and original data cannot be achieved, because our calculation is based on the integrated J_{sc} from the quantum efficiency whereas most publications work with the *JV* measurement data. Additionally, we remark to check the correct calculation of the efficiency, because in some data the simple equation $\eta = J_{\mathrm{sc}} V_{\mathrm{oc}} FF / P_{\mathrm{in}}$ does not hold true or it is not clear from which parameters the efficiency is calculated. If all data is measured precisely at a defined illumination, theoretical values and the original data must match well. Therefore, this method also gives the chance to validate low light measurements and editors or reviewers can judge whether some data credibly reports a certain efficiency under a certain illumination condition. Note that optical ND filters, which may be used to achieve sufficiently low light intensities, have (unlike what the name suggests) a wavelength-dependent transmission which varies mostly at the edge of the visible spectrum. Thus, in particular the region $\lambda > 700$ nm becomes problematic, because at these wavelengths many organic solar cells for indoor applications will still absorb light well. The spectral dependencies of ND filters will cause changes in the spectra if used in low light set-ups and will therefore affect P_{out} but more importantly P_{in} @ 200 lux and the efficiency.

As there are inconsistencies for a huge amount of publications, this emphasizes the need of a reliable comparison method. Even if the concept of efficiencies would be omitted to circumvent the determination of the input power, the output power is heavily dependent on the illumination. The output power may be measured correctly, but if the illumination is wrongly determined the comparison of publications is impossible due to the shift of the lux axis. Therefore, we strongly recommend the comparison with calculated values based on the spectra and the quantum efficiency as this method does not only verify the measured values, but also enables a high level of comparability between different labs, setups and light sources.

3.2 Influence of LEDs with different photon energies on the performance of indoor solar cells

Publications use different LEDs with varying photon energies to examine the performance of iPVs. Different photon energies affect the efficiency of solar cells by the direct influence on the input power. Furthermore, the solar cells' $Q_{\mathrm{e,PV}}$ onset should be suitable for a certain type of LED, so that an optimal absorption of the incoming light over all wavelengths is ensured.

Firstly, we discuss the case for perfect absorption by applying a modified version of the Shockley-Queisser[74] model based on the principal of detailed balance[75] to different LED spectra. Freunek et al. had previously presented a calculation for different types of light sources, but at a constant irradiance[76] and Ho et al. had presented calculations which mainly focused on the influence of different illuminances.[77] Similar calculations were performed for other technologies[52] or used empirical approaches[78–80]. Here, in contrast to Freunek et al., we examine the influence of different LED light sources at constant illuminance instead of the constant irradiance calculation done by Freunek et al. The detailed balance model assumes a single abrupt absorption onset, i.e. in mathematical terms a step-function like absorptance of the absorber layer that is zero below the band gap and one above the band gap. This idealization is a sensible upper limit for efficiency and different solar cell technologies come differently

close to an abrupt absorption onset. Early generations of organic solar cells featured substantial losses[81,82] due to non-abrupt absorption onsets caused by the different absorption feature of the donor, the acceptor and the charge transfer state. Therefore, variants of the detailed balance model with Gaussian[83], exponential[84] or multistep-absorption onsets[85] were devised. The efficiency improvements in recent generations of organic solar cells have however led to substantially steeper absorption onsets[86,87] and smaller differences between donor, acceptor and CT state absorption features[88,89]. These developments imply that the original Shockley-Queisser model becomes more relevant with the continuous improvement of OPV efficiencies and motivates our use of the traditional step-function. In addition to the step-function absorptance, the detailed balance model also idealizes the contacts (no resistive losses), transport (all photogenerated electron hole pairs are collected) and recombination (only radiative recombination is included in the model). In reality, losses will occur due to imperfect contacts, finite mobilities and due to non-radiative recombination and thereby lead to lower than optimum efficiencies. A detailed description of the performed calculation can be found in the supplementary information.

In **Figure 4**(a) the spectra of LEDs with different photon energies are depicted, which were normalized to 200 lux as described above. The LED of Ding et al. shows the highest photon energies with a main peak at ~450 nm. As the LEDs decrease in color temperature, the main peak decreases and the other peak gets more pronounced. The LED with 2700 K used in our group exhibit the lowest photon energies and shows a main peak around ~640 nm. Note that the color temperatures given by the manufacturer are insufficient to characterize the spectra. We found different color temperatures (stated by the manufacturer) for similar spectra in literature as well as identical color temperatures for different spectra. In Figure 4(b) the integrated irradiances are shown. The values at 800 nm are the input power densities of the LED. At a constant illuminance, LEDs with spectra close to the $V(\lambda)$ maximum at 555 nm (such as the 4100 K LED) need less input power for a certain illuminance. Consequently, P_{in}

is decreasing from LEDs with high photon energies to the 4100 K LED as the spectra shift closer to the $V(\lambda)$ maximum. Subsequently, P_{in} increases for the 2700 K LED of Cui et al. and the 2700 K LED of our group as more input power is needed to reach the constant illuminance of 200 lux.

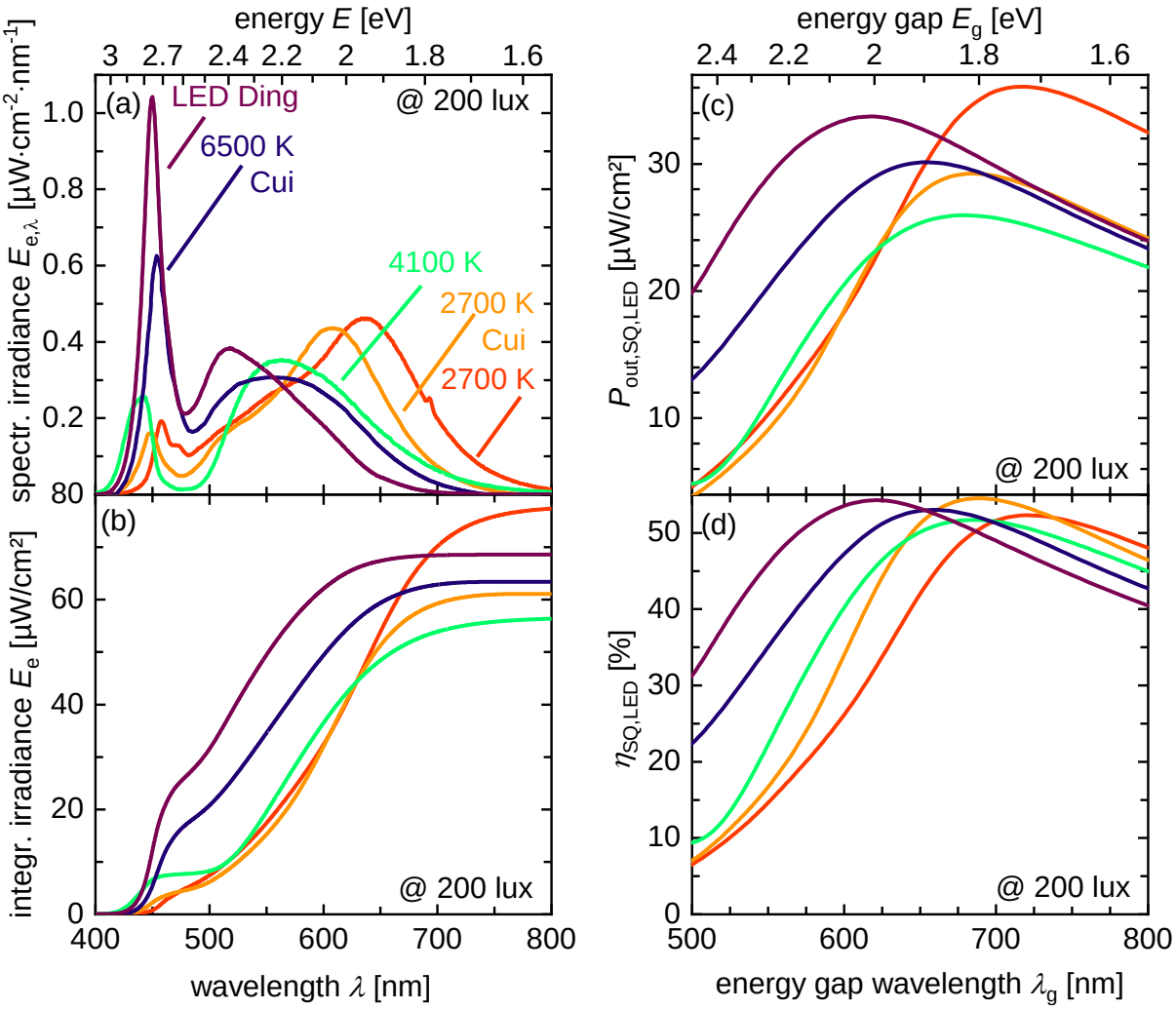

Figure 4. (a) Spectral irradiance and (b) integrated irradiance data for a selection of LEDs (LED Ding from Ref. [33], LED 6500 K and LED 2700 K from Ref. [30] and LED 4100 K and 2700 K are from our group). The spectra were normalized to 200 lux as described above. For the input spectra the output power $P_{\mathrm{out,SQ,LED}}$ (c) and the efficiency $\eta_{\mathrm{SQ,LED}}$ (d) within the adapted Shockley-Queisser model were calculated. The maximum output power is following the input power as all LED spectra were normalized to a constant illuminance of 200 lux.

With the spectra normalized to 200 lux, the performance parameters were calculated within the Shockley-Queisser model. In Figure 4(c) and 4(d) the resulting output power densities $P_{\mathrm{out,SQ,LED}}$ and the efficiency $\eta_{\mathrm{SQ,LED}}$ are depicted, respectively. All other performance parameters can be found in Figure S10. For the LED of Ding et al., the maximum $P_{\mathrm{out,SQ,LED}}$ of 33 µW/cm² is found for materials with a band gap of 2 eV. With decreasing LED photon energies, the maximum $P_{\mathrm{out,SQ,LED}}$ is decreasing as the input power is decreasing. The maximum output power of the LED with 4100 K is shifted to band gaps of 1.8 eV and amounts to 26 µW/cm². Subsequently, with decreasing photon energies the $P_{\mathrm{out,SQ,LED}}$ is increasing again and reaches its maximum of 36 µW/cm² for the 2700 K LED with a band gap of 1.7 eV. Hence, the maximum output power is strongly affected by the spectrum of the LED. Spectra close to the $V(\lambda)$ maximum of 555 nm have lower output powers for the situation of constant illuminances. As we pointed out in section 2.2, the spectra of different LED have a strong influence on the efficiency of the solar cell. Our calculations are done with different LED spectra compared to the existing ones in literature, implying that we will not get identical but only similar results. For instance, the spectrum of the 2700 K LED of Cui et al. resembles the 3000 K LED spectrum of Ho et al.[77] (Table S1(b) in the reference) and hence leads to similar efficiency values in the modified SQ model. Ho et al. state an input power of 59.6 µW at 200 lux with an optimal absorber band gap of 1.83 eV and a maximum efficiency of 53.24 %, which are in good agreement with our results (input power of 60.7 µW/cm², optimal absorber band gap of 1.80 eV and a maximum efficiency of 54.4 %). The results of other LEDs used by Ho et al. differ slightly due to slightly different input spectra.

To investigate the effect of LED spectra on actual organic solar cells, a selection of well-performing solar cells with different absorption band onsets were investigated. Note, that although in this study we focus on OPV, our method is applicable to all solar cell technologies. The $Q_{\mathrm{e,PV}}$ of the solar cells can be found in Figure S11 and the wavelength of the band gap λ_{g}

was determined by finding the inflection point of the $Q_{\mathrm{e,PV}}$ data.[90] The values of λ_{g} are 644 nm, 675 nm, 702 nm and 803 nm for the CD1:PBN-10 (Ding et al., Ref. [33]), PBDB-TF:IO-4Cl (Cui et al., Ref. [31]), PBDB-TF:ITCC (Cui et al., Ref. [30]), and the PM6:Y6-O (Ma et al., Ref. [35]) solar cell, respectively. As the λ_{g} is increasing, the color code in **Figure 5** changes from orange to brown. High band gap samples typically reach lower short circuit current densities and higher open-circuit voltages than lower band gap solar cells, and vice versa for low band gap materials. For each LED spectrum, there is an optimal band gap that minimizes losses in J_{sc} (i.e. non-absorption losses) and V_{oc} (i.e. thermalization and recombination losses) such that we achieve the maximum efficiency. As this influence shifts the absolute efficiency, all parameters and the input power of the LEDs shown in Figure 5 were normalized to the values of the LED with 2700 K. Hence, we can investigate the relative influence of different LED spectra on the performance parameters. The x-axis of Figure 5 is sorted from LEDs with high to low color temperature from left to right (i.e. cold white to warm white). The first (second) region with higher (lower) photon energy LEDs is marked with blue (red) rectangles as guide to the eye. Absolute values as well as the V_{oc} and FF dependence are displayed in Figure S12.

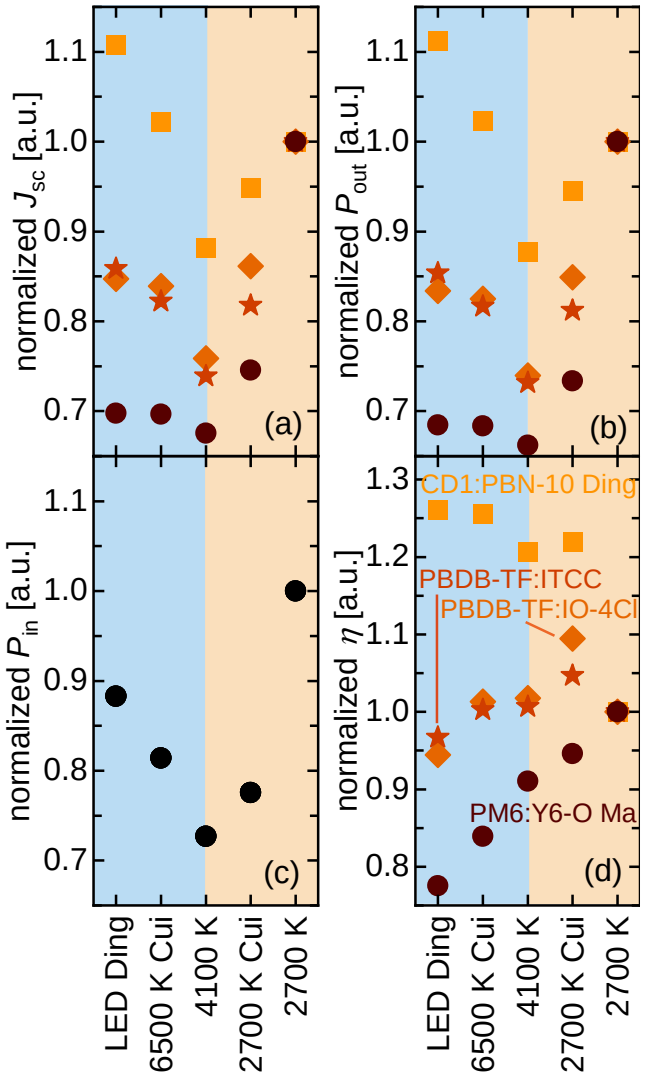

Figure 5. Performance parameters of highly efficient solar cells with varying onset λ_g of the quantum efficiency $Q_{e,PV}$ performing under different LED light sources with constant illumination of 200 lux. The colors change from yellow to brown for samples with increasing λ_g of the $Q_{e,PV}$. The J_{sc} (a), the P_{out} (b), the P_{in} (c) and the η (d) were normalized to the results of the 2700 K LED with lowest photon energies. Samples with high band gaps (low λ_g, orange symbols) are better performing with high color temperature LEDs and samples with low band gaps (higher λ_g, brown symbols) excel for LEDs with lower color temperature. Note, that due to the normalization to the LED with 2700 K all points overlay for the LED with 2700 K.

Figure 5 shows the normalized J_{sc}, P_{out}, P_{in}, and η, respectively. All four parameters vary by about 15 % to 25% due to the different overlap of the LED spectra with the eye sensitivity and the solar cell quantum efficiencies. Depending on the absorber material, the efficiency may increase (e.g. low band gap material PM6:Y6-O) or decrease (e.g. high band gap material

CD1:PBN-10) with decreasing color temperature, indicating that low band gap materials perform better with low color temperature LEDs and vice versa (Figure 4(d)). The color temperature dependence of the efficiency implies that any ranking or comparison of indoor solar cells strongly depends on the used LED.

We conclude, that the performance of iPV depends on the delicate interplay between the spectral irradiance of the LED and the quantum efficiency $Q_{\mathrm{e,PV}}$ of the solar cell. LEDs with spectra close to the luminous efficacy curve exhibit lower input powers, which decrease the output power. The efficiency dependence on the LEDs color temperature is changing with the band gap of the absorber material. For high band gaps, a high color temperature LED is more suitable and for materials with low band gaps, a LED with low color temperature is performing better.

3.3 Comparing efficiencies of different publications

Comparing efficiencies of different publications is hard to handle fairly due to the variety of light sources and used illumination intensities. This problem is widely known and discussed in literature[31,51,59,62,91] and studies of Cui et al. depicted origins of measuring errors and developed measuring protocols. Nevertheless, the problem of comparing data generated with different light source spectra still remains. With our presented method we can rank photovoltaic cells across literature for the first time, although the original data was measured under one specific light source. In the following this is exemplarily shown for OPV technology.

As we have seen above, different LED spectra favor different blends with varying absorption onsets thereby complicating any fair comparison between literature data. Thus, we propose to compare and rank efficiencies and output powers @200 lux by choosing the best LED for each solar cell. The “best” LED means the one which leads to the highest efficiency under an illuminance of 200 lux.

Firstly, the calculation was carried out for a wide set of data from literature[16–19,30–35] for the whole set of different LEDs presented above with a constant illuminance of 200 lux. Unfortunately, some high-performance solar cells could not be included due to lack of necessary data. To get an overview, only the performance parameters for each sample resulting from the LED irradiation with the best efficiency are considered. The threshold efficiency for inclusion in the study was 10% at 200 Lux under at least one of the 5 LED spectra shown in Figure 4a. In **Figure 6** the performance parameters are plotted against the publications with increasing efficiency. All samples which reached the best efficiency with the LED of Ding et al, the LED with 2700 K of Cui et al. and the LED with 2700 K used in our work, are displayed in purple, orange and red color, respectively. In Table S1 and S2 the parameters are listed and the materials and references can be found as well.

This comparison also includes two absorber blends fabricated in our group. The high band gap blend PDBD-T:F-M and the low band gap blend PBDB-TF-T1:Y12 are fabricated with the green solvent o-xylol and the 0.16 cm² devices exhibit an active layer area thickness of around 190 nm and 180 nm, respectively, which is higher than optimal for one-sun performance. For the PBDB-T:F-M device the performance under 1 sun illumination was relatively poor with a J_{sc} of 12.4 mA/cm² a V_{oc} of 0.89 V and a FF of 49.9 %, leading to an efficiency of 5.5 %. With an efficiency of 12.2 %, the PBDB-TF-T1:Y12 device strongly outperformed the PBDB-T:F-M solar cell under 1 sun illumination with a J_{sc} of 24.4 mA/cm², a V_{oc} of 0.84 V and a FF of 59.5 %. All JV and $Q_{e,PV}$ measurements can be found in Figure S13 and performance parameters for 1 sun and low light illumination are listed in Table S3 and S4. Figure 6 illustrates, that under an illumination of 200 lux the PBDB-T:F-M (2700 K LED, Lueb 2. in Figure 6) and the device PBDB-TF-T1:Y12 (2700 K LED Cui, Lueb. 1 in Figure 6) reach efficiencies of 13.5 % and 12.9 %. This example manifests, that devices, which perform poorly under for 1 sun conditions, can be well performing in the low light regime

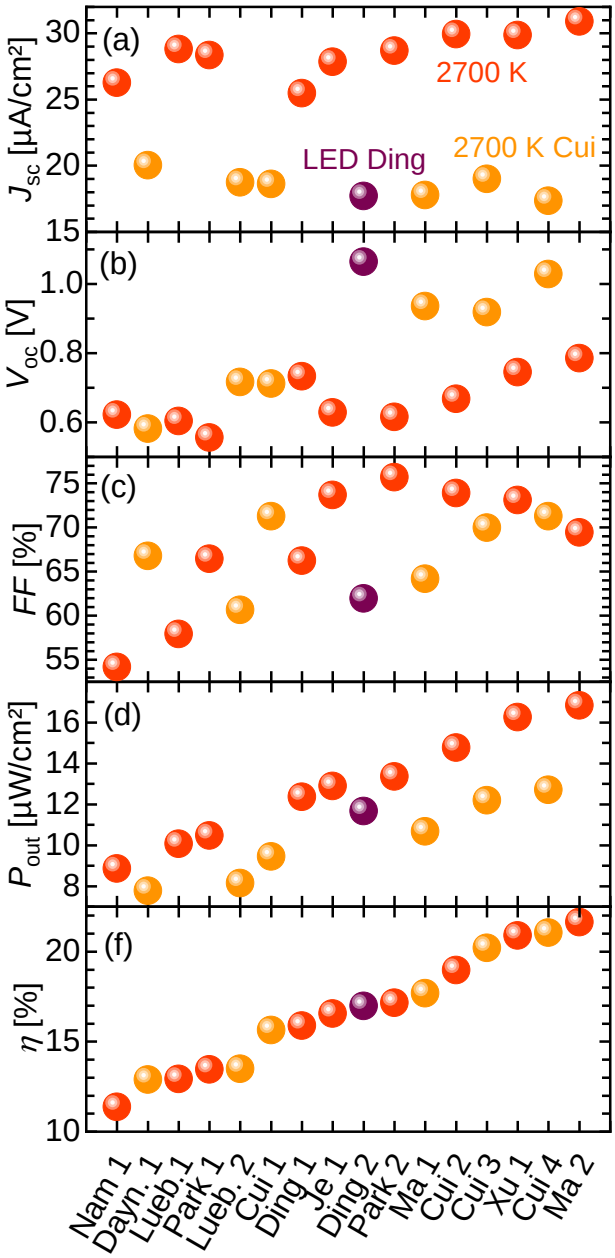

Figure 6. Performance parameters of the analyzed samples are displayed and sorted by increasing efficiency on the x-axis. To rank the efficiencies, the calculation was done for the whole set of 5 LEDs, but only the highest resulting efficiency is shown. Efficiencies resulting from illumination with the LED of Ding et al, the LED with 2700 K of Cui et al. and the LED with 2700 K used in our work, are displayed in purple, orange and red color, respectively. Materials of one publication are numbered and the specific material of the respective publication can be found in Table S1 in the supporting information.

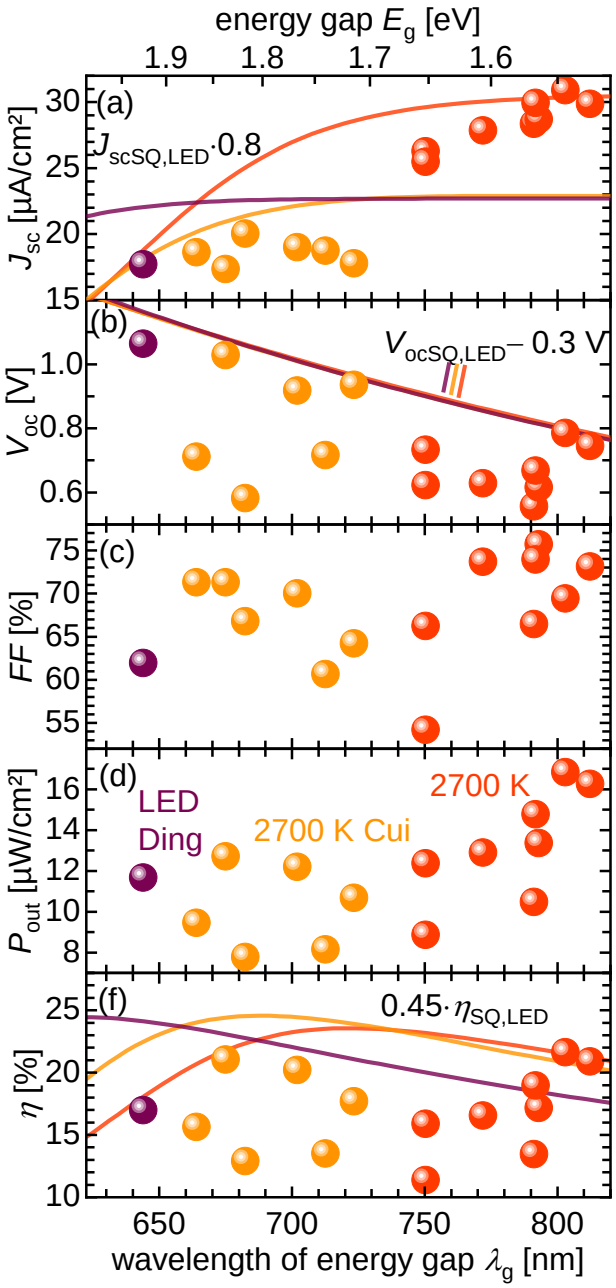

Figure 7. Performance parameters of a wide range of samples from literature plotted against the wavelength of the band gap. Specific information about the materials and publications can be found in Table S2. Straight lines with colors of the respective LED light source are shown to indicate the trends of the maximum performance (modified Shockley-Queisser model). Note, that the lines are adjusted with arbitrary constants to better fit the experimental data, so that the lines fulfill their purpose as guide to the eye. The J_{sc} was adjusted to 80 % of the maximum J_{sc} and the efficiency to 45 % of its maximum. Furthermore, we subtracted 0.3 V from the maximum V_{oc} to better match the values. Note that the V_{oc} lines for the different LEDs overlap as they only depend weakly on the used LED source.

In **Figure 7** the performance parameters are plotted against the band gap wavelength λ_g . In accordance to the Shockley-Queisser model, materials with lower band gaps exhibit higher short circuit current densities J_{sc} and lower open-circuit voltages V_{oc}. The efficiency peaks around band gap wavelengths of ~675 nm (~1.84 eV) for the illumination with the 2700 K LED of Cui et al.. The maximum for the illumination with the 2700 K LED used in our group is located around a band gap wavelength of ~800 nm (~1.55 eV).

To illustrate if these maxima are in accordance to the Shockley-Queisser calculation, in **Figure 8** the efficiencies of our meta-analysis as well as the maximum efficiencies from the Shockley-Queisser calculation are plotted. Straight lines exhibit the maximum Shockley-Queisser efficiencies for the different input LED spectra. Dashed lines incorporate an additional, non-radiative voltage loss of 180 meV representative of the lowest reported values in the literature that are in the range of 0.16 V-0.2 V.[88,92,93]

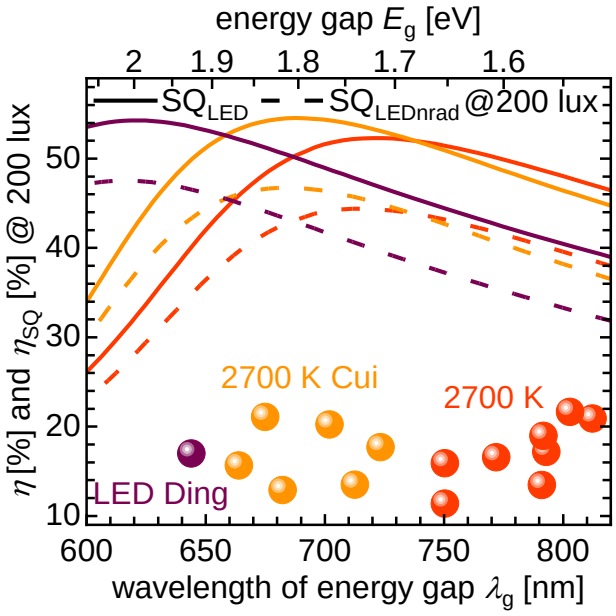

Figure 8. Efficiencies resulting from our calculations for a constant illuminance of 200 lux for a wide set of iOPV devices from literature (dots). Straight lines show the Shockley-Queisser efficiencies resulting from illumination of the LED of Ding et al. (purple), the 2700 K LED of Cui et al. (orange) and the 2700 K LED used in our group (red). Efficiencies resulting from Shockley-Queisser calculations with a non-radiative voltage loss of 180 meV are depicted in dashed lines.

For the samples, which reached the best efficiencies with the 2700 K LED of Cui et al., the peak around 1.84 eV is overlapping with the position of the Shockley-Queisser maximum, suggesting the band gap to be suitable for this LED illumination. Theoretically, with this kind of LED spectrum a maximum efficiency of 54 % is possible, emphasizing the potential for further improvements. Interestingly, the best experimental efficiencies for the 2700 K LED at 1.55 eV (red symbols compared to red line) do not coincide with the Shockley-Queisser maximum of 1.7 eV. This could imply that the electronic quality of the materials dominates the optimum band gap for the experimental data. All in all, this detailed analysis manifests the state of the art for iOPV and shows that there is still substantial room for improvement for all three PV parameters (J_{sc}, V_{oc} and *FF*).

4. Conclusion

In this work, we proposed a method, which enables the calculation of efficiencies at a fixed illumination level based on simple standard measurements as *JV* and quantum efficiency measurements. The possibility to scan the performance for different LED emission spectra and light intensities, ensures a fair comparison between PV publications as the arbitrariness of low light setups is inevitable. While our method is applicable to any solar cell technology, where J_{sc} can be precisely determined from the external quantum efficiency, we apply our method to organic solar cells whose data are either measured in house or taken from literature. Firstly, we validated our evaluation method thoroughly and showed that about 65 % of the efficiencies studied from literature are in good agreement with our model. The other 35 % showed total deviations of the absolute efficiency >3 %, including some absolute efficiencies deviating ~8 %. These deviations stress the need for consistency checks of low light efficiencies using quantum efficiency data and LED spectra to support the current voltage curves. Furthermore, we demonstrated quantitively the delicate dependence of the output power and the efficiency of iOPVs on the LED spectra. The efficiencies are governed by the overlap of the quantum

efficiency and the LED spectrum and vary by ± 20 %-25 % when using different LED spectra depending on the absorber band gap. Calculations with an ideal absorber within the Shockley-Queisser limit with a fixed illumination of 200 lux completed this study and emphasized that there is still substantial room for improvement of this technology as the maximum Shockley-Queisser efficiency is 52 % - 54 % depending on the used LED spectrum. The optimal band gap of the absorber depends on the LEDs' spectrum and is ranging between 1.75 eV and 2 eV. Finally, we analyzed a wide set of different iOPVs from literature and rank them according to their efficiency under the LED that fits each cell best. This fair comparison shows that the presented calculation is a powerful tool to detect possible candidates for high indoor performance solar cells for an arbitrary light source.

5. **Experimental section/methods**

Stepwise calculation of η:

In the first step the input power of the light source is determined (section 2.1). The relative spectral irradiance $E_{\mathrm{e},\lambda,\mathrm{ref}}$ data is supposed to be in units of W/m²/nm and can be measured by a spectrometer. The spectral illuminance $E_{\mathrm{v},\lambda,\mathrm{ref}}$ is calculated by Equation 2. Integration of the relative spectral irradiance $E_{\mathrm{e},\lambda,\mathrm{ref}}$ and the spectral illuminance $E_{\mathrm{v},\lambda,\mathrm{ref}}$ leads to the reference irradiance $E_{\mathrm{e,ref}}$ and the reference illuminance $E_{\mathrm{v,ref}}$. Then, the factor f for a certain illuminance (e.g. 200 lux) is calculated with $f_{200\,\mathrm{lux}} = 200\,\mathrm{lux}/E_{\mathrm{v,ref}}$ (Equation 4), leading to one factor for each illuminance level. The irradiance at the chosen illuminance level can be calculated with $P_{\mathrm{in}} = f_{200\,\mathrm{lux}} \cdot E_{\mathrm{e,ref}}$ (Equation 5). After multiplying $E_{\mathrm{e},\lambda,\mathrm{ref}}$ with the factor $f_{200\,\mathrm{lux}}$, the relative spectral irradiance data is normalized to the desired illuminance and the determination of the light sources' input power is done.

In the second step the output power of the solar cell is adjusted (section 2.2). The short circuit current density is calculated by Equation 6, using the normalized spectral irradiance data.

The $V_{oc}(J_{sc})$ and $FF(J_{sc})$ data is gained by *JV* measurements close to the desired lux levels with any light source. Then, the exact V_{oc} and FF values are determined by a 'pchip' interpolation. Linear interpolation should obtain similar results, but the 'pchip' interpolation proved to match better results in case of considering whole ranges of illuminance levels (from 200 to 10^5 lux) or in case of extrapolation to smaller J_{sc} (calculated J_{sc} from $Q_{e,PV}$ smaller than measured J_{sc} from *JV*). Now $P_{out} = J_{sc} \cdot V_{oc} \cdot FF$ gives the output power and with the input power of section 2.1 the efficiency can be calculated. The *Matlab* code can be found on https://github.com/tkirchartz/Determine_Indoor_PV_Performance.

Device fabrication:

First, a structured indium tin oxide (ITO) layer (~150 nm) on glass a substrate is cleaned in an ultrasonic cleaner for 10 minutes in distilled water, acetone and isopropyl alcohol, respectively. The substrates are dried at 100 °C on a hotplate and treated with an oxygen plasma. For the PBDB-T:F-M samples the device structure is ITO/ZnO/blend/MoO_x/Ag and for the PBDB-TF-T1:BTP-4F-12 (PBDB-TF-T1:Y12) samples the device structure is ITO/PEDOT:PSS/blend/PFN-Br/Ag.

For the PBDB-T:F-M devices, the zinc oxide (ZnO) interlayer is processed from a sol-gel. 100 mg of zinc acetate dihydrate (*Sigma Aldrich*), 1.5 ml 2-methoxyethanol (*Alfa Aesar*) and 28 µL ethanol amine (*Sigma Aldrich*) are stirred at 60 °C overnight and filtered with a 0.45 µm PVDF filter. The ZnO sol-gel is spin-coated on top of the ITO with 6000 rpm for 50 s and is annealed at 200 °C for 20 minutes, resulting in a ZnO layer of ~30 nm. The devices were transferred into a glovebox for further preparation.

The polymer **PBDB-T** *Poly[[4,8-bis[5-(2-ethylhexyl)-2-thienyl]benzo[1,2-b:4,5-b']dithiophene-2,6-diyl]-2,5-thiophenediyl[5,7-bis(2-ethylhexyl)-4,8-dioxo-4H,8H-benzo[1,2-c:4,5-c']dithiophene-1,3-diyl]]* and the NFA **F-M** *4,4,7,7,12,12-octyl-7,12–dihydro–bis [ethylidyne(3-oxo-methyl-1Hindene-2,1(3H)-diylidene)]]bis-4H-thieno[2",3":1',2']indeno*

[5',6':5,6]-s-indaceno[1,2-b]thiophenein were purchased from *1-material*. PBDB-T and F-M were dissolved with a 1:1 ratio and a concentration of 17 mg/ml in ortho-xylene (o-xylene). The solution was stirred overnight at 100 °C in the glovebox and prior to spin-coating 0.2 % of 1,8-diiooctane (DIO) was added. The solution was spin-coated dynamically with a speed of 1000 rpm and 3000 rpm for 40 s to obtain an active layer with thicknesses of ~190 nm and ~100 nm, respectively. Thicknesses were estimated with capacitance measurements as described below. Finally, 8 nm of MoO_x and ~100 nm silver (Ag) were evaporated under high vacuum (~5×10−7 mbar). The device area was defined by a shadow mask and is 0.16 cm² for devices for 1 sun *JV* and Q_e measurements and 0.06 cm² for devices for measurements of $V_{oc}(J_{sc})$ and $FF(J_{sc})$ pairs in the low light regime.

For the PBDB-TF-T1:Y12 samples, *Poly(3,4-ethylenedioxythiophene) polystyrene sulfonate* PEDOT:PSS Al 4083 from *Ossila* was treated with an ultrasonic cleaner under cooling for 15 min before filtering with a 0.45 µm PDVF filter. The PEDOT:PSS was spin-coated at 4000 rpm for 30 s and then annealed at 150 °C for 20 minutes. The substrates were subsequently transferred into a nitrogen atmosphere. For the active layer, the donor **PBDBT-TF-T1** *Poly[(2,6-(4,8-bis(5-(2-ethylhexyl-3-fluoro)thiophen-2-yl)-benzo[1,2-b:4,5-b']dithiophene))-alt-(5,5-(1',3'-di-2-thienyl-5',7'-bis(2-ethylhexyl)benzo[1',2'-c:4',5'-'] dithiophene-4,8-dione)]*-ran-*poly[(2,6-(4,8-bis(5-(2-ethylhexyl)thiophen-2-yl)-benzo[1,2-b:4,5-b']dithiophene))-alt-(2,2-ethyl-3(or4)-carboxylate-thiophene)]* and the NFA **BTP-4F-12** *2,2'-((2Z,2'Z)-((12,13-bis(2-butyloctyl)-3,9-diundecyl-12,13-dihydro-[1,2,5] thiadiazolo[3,4-e]thieno[2'',3'':4',5']thieno[2',3':4,5]pyrrolo[3,2-g]thieno[2',3':4,5]thieno[3,2-b]indole-2,10-diyl)bis(methanylylidene))bis(5,6-difluoro-3-oxo-2,3-dihydro-1H-indene-2,1-diylidene)) dimalononitrile* (Y12) (purchased from *1-material*) were dissolved with a ratio 1:1.2 in o-xylene with a concentration of 25 mg/ml and stirred at room temperature about 3 h before spin-casting. The solution was spin-coated dynamically with 2800 rpm for 30 s and annealed at 100 °C for 10 min, resulting in an active layer thickness ~180 nm. PFN-Br was dissolved in

methanol with a concentration of 0.5 mg/ml, filtered with a 0.45 µm PDVF filter and spin-coated on top of the active layer dynamically with 2500 rpm for 30 s. Finally, 100 nm Ag were evaporated under high vacuum (~5×10−7 mbar). The device area was defined by a shadow mask and is 0.16 cm².

Device characterization:

JV measurements under 1 sun irradiation were performed with solar simulator from *LOT Quantum Design* and a *Keithley 2450* was used as the source meter. As the samples are measured in a sealed box and the incident light is reflected two times at the glass window, current densities are corrected with additional 8 %. Capacitance measurements were performed with a potentiostat *Interface 1000* by the company *Gamry Instruments* to estimate thicknesses of the active layer in a non-destructive way. For this estimation the capacitance at high negative voltages (-3 V) was determined in the dark and a permittivity ε_r of 3.9 was used. For low light measurements a warm white LED (CXA3050-0000-000N0YU227H) by the company *Cree* is used as a light source. According to manufacturer information the color temperature is 2700 K. To estimate the illumination for the *JV* measurements (which give the $V_{oc}(J_{sc})$ and $(FF)J_{sc}$ pairs for the interpolation) a lux meter MS-200LED of the company *Voltcraft* is used. We emphasize that the lux meter is only used for a rough estimation of the illuminance level and not to calculate efficiencies. The quantum efficiency measurements were performed with a home-made setup. A *BENTHAM* 605 lamp power supply powers the halogen and xenon lamp. A monochromator TM300 of the company *BENTHAM* has a symmetric Czerny-Turner geometry and uses diffraction gratings. As well as for the *JV* measurements the current densities from Q_e measurements are also corrected with 8 % refraction losses.

Acknowledgements
We acknowledge funding for the project Enerscale from the state Nordrhein-Westfalen and the European Union (via the European Fonds for Regional Development). Furthermore, we acknowlege funding from the Helmholtz Association. The authors declare no competing interest.

References:

[1] Y. Cui, H. Yao, J. Zhang, T. Zhang, Y. Wang, L. Hong, K. Xian, B. Xu, S. Zhang, J. Peng, Z. Wei, F. Gao, J. Hou, *Nat. Commun.* **2019**, *10*, 2515.

[2] Y. Cui, H. Yao, J. Zhang, K. Xian, T. Zhang, L. Hong, Y. Wang, Y. Xu, K. Ma, C. An, C. He, Z. Wei, F. Gao, J. Hou, *Adv. Mater.* **2020**, *32*, 1908205.

[3] Y. Lin, Y. Firdaus, F. H. Isikgor, M. I. Nugraha, E. Yengel, G. T. Harrison, R. Hallani, A. El-Labban, H. Faber, C. Ma, X. Zheng, A. Subbiah, C. T. Howells, O. M. Bakr, I. McCulloch, S. De Wolf, L. Tsetseris, T. D. Anthopoulos, *ACS Energy Lett.* **2020**, *5*, 2935.

[4] Q. Liu, Y. Jiang, K. Jin, J. Qin, J. Xu, W. Li, J. Xiong, J. Liu, Z. Xiao, K. Sun, S. Yang, X. Zhang, L. Ding, *Sci. Bull.* **2020**, *65*, 272.

[5] Y. Lin, M. I. Nugraha, Y. Firdaus, A. D. Scaccabarozzi, F. Aniés, A.-H. H. Emwas, E. Yengel, X. Zheng, J. Liu, W. Wahyudi, E. Yarali, H. Faber, O. M. Bakr, L. Tsetseris, M. Heeney, T. D. Anthopoulos, *ACS Energy Lett.* **2020**, *5*, 3663.

[6] Y. Cui, H. Yao, L. Hong, T. Zhang, Y. Tang, B. Lin, K. Xian, B. Gao, C. An, P. Bi, W.

Ma, J. Hou, *Natl. Sci. Rev.* **2020**, *7*, 1239.

[7] O. Almora, D. Baran, G. C. Bazan, C. Berger, C. I. Cabrera, K. R. Catchpole, S. Erten-Ela, F. Guo, J. Hauch, A. W. Y. Ho-Baillie, T. J. Jacobsson, R. A. J. Janssen, T. Kirchartz, N. Kopidakis, Y. Li, M. A. Loi, R. R. Lunt, X. Mathew, M. D. McGehee, J. Min, D. B. Mitzi, M. K. Nazeeruddin, J. Nelson, A. F. Nogueira, U. W. Paetzold, N. Park, B. P. Rand, U. Rau, H. J. Snaith, E. Unger, L. Vaillant-Roca, H. Yip, C. J. Brabec, *Adv. Energy Mater.* **2021**, *11*, 2002774.

[8] J. Gubbi, R. Buyya, S. Marusic, M. Palaniswami, *Futur. Gener. Comput. Syst.* **2013**, *29*, 1645.

[9] L. Atzori, A. Iera, G. Morabito, *Comput. Networks* **2010**, *54*, 2787.

[10] A. Al-Fuqaha, M. Guizani, M. Mohammadi, M. Aledhari, M. Ayyash, *IEEE Commun. Surv. Tutorials* **2015**, *17*, 2347.

[11] H. Jayakumar, K. Lee, W. S. Lee, A. Raha, Y. Kim, V. Raghunathan, in *Proc. 2014 Int. Symp. Low Power Electron. Des.*, ACM, New York, NY, USA, **2014**, pp. 375–380.

[12] I. Mathews, S. N. Kantareddy, T. Buonassisi, I. M. Peters, *Joule* **2019**, *3*, 1415.

[13] H. Yu, Q. Yue, *Energy Procedia* **2012**, *16*, 1027.

[14] H. K. H. H. Lee, Z. Li, J. R. Durrant, W. C. Tsoi, *Appl. Phys. Lett.* **2016**, *108*, 253301.

[15] H. K. H. Lee, J. Wu, J. Barbé, S. M. Jain, S. Wood, E. M. Speller, Z. Li, F. A. Castro, J. R. Durrant, W. C. Tsoi, *J. Mater. Chem. A* **2018**, *6*, 5618.

[16] M. Nam, H. Y. Noh, J. Cho, Y. Park, S. Shin, J. Kim, J. Kim, H. H. Lee, J. W. Shim, D. Ko, *Adv. Funct. Mater.* **2019**, *29*, 1900154.

[17] S. Park, H. Ahn, J. J. Y. J. J. Y. J. Kim, J. B. Park, J. J. Y. J. J. Y. J. Kim, S. H. Im, H. J. Son, *ACS Energy Lett.* **2020**, *5*, 170.

[18] Y. Xu, H. Yao, L. Ma, Z. Wu, Y. Cui, L. Hong, Y. Zu, J. Wang, H. Y. Woo, J. Hou, *Mater. Chem. Front.* **2021**, *5*, 893.

[19] H. Yin, L. Ma, J. Yan, Z. Zhang, A. M. H. Cheung, J. Zhang, H. Yan, S. K. So, *Sol.*

RRL **2020**, *4*, 2000291.

[20] R. Arai, S. Furukawa, Y. Hidaka, H. Komiyama, T. Yasuda, *ACS Appl. Mater. Interfaces* **2019**, *11*, 9259.

[21] C. H. Chen, H. C. Ting, Y. Z. Li, Y. C. Lo, P. H. Sher, J. K. Wang, T. L. Chiu, C. F. Lin, I. S. Hsu, J. H. Lee, S. W. Liu, K. T. Wong, *ACS Appl. Mater. Interfaces* **2019**, *11*, 8337.

[22] C. Y. Liao, Y. Chen, C. C. Lee, G. Wang, N. W. Teng, C. H. Lee, W. L. Li, Y. K. Chen, C. H. Li, H. L. Ho, P. H. S. Tan, B. Wang, Y. C. Huang, R. M. Young, M. R. Wasielewski, T. J. Marks, Y. M. Chang, A. Facchetti, *Joule* **2020**, *4*, 189.

[23] J. Liu, Y. Cui, Y. Zu, C. An, B. Xu, H. Yao, S. Zhang, J. Hou, *Org. Electron.* **2020**, *85*, 105798.

[24] J. Luke, L. Corrêa, J. Rodrigues, J. Martins, M. Daboczi, D. Bagnis, J. Kim, *Adv. Energy Mater.* **2021**, *11*, 2003405.

[25] S.-C. Shin, C. W. Koh, P. Vincent, J. S. Goo, J.-H. Bae, J.-J. Lee, C. Shin, H. Kim, H. Y. Woo, J. W. Shim, *Nano Energy* **2019**, *58*, 466.

[26] H. Yin, J. K. W. Ho, S. H. Cheung, R. J. Yan, K. L. Chiu, X. Hao, S. K. So, *J. Mater. Chem. A* **2018**, *6*, 8579.

[27] R. Singh, C. L. Chochos, V. G. Gregoriou, A. D. Nega, M. Kim, M. Kumar, S. C. Shin, S. H. Kim, J. W. Shim, J. J. Lee, *ACS Appl. Mater. Interfaces* **2019**, *11*, 36905.

[28] R. Singh, T. Duan, Z. Kan, C. L. Chochos, G. P. Kini, M. Kumar, J. Park, J. Lee, J.-J. Lee, *Nano Energy* **2020**, *75*, 104934.

[29] Y. You, C. E. Song, Q. V. Hoang, Y. Kang, J. S. Goo, D. Ko, J. Lee, W. S. Shin, J. W. Shim, *Adv. Funct. Mater.* **2019**, *29*, 1901171.

[30] Y. Cui, H. Yao, T. Zhang, L. Hong, B. Gao, K. Xian, J. Qin, J. Hou, *Adv. Mater.* **2019**, *31*, 1904512.

[31] Y. Cui, Y. Wang, J. Bergqvist, H. Yao, Y. Xu, B. Gao, C. Yang, S. Zhang, O. Inganäs,

F. Gao, J. Hou, *Nat. Energy* **2019**, *4*, 768.

[32] S. V. Dayneko, M. Pahlevani, G. C. Welch, *ACS Appl. Mater. Interfaces* **2019**, *11*, 46017.

[33] Z. Ding, R. Zhao, Y. Yu, J. Liu, *J. Mater. Chem. A* **2019**, *7*, 26533.

[34] H. Il Je, E. Y. Shin, K. J. Lee, H. Ahn, S. Park, S. H. Im, Y. H. Kim, H. J. Son, S. K. Kwon, *ACS Appl. Mater. Interfaces* **2020**, *12*, 23181.

[35] L. K. Ma, Y. Chen, P. C. Y. Y. Chow, G. Zhang, J. Huang, C. Ma, J. Zhang, H. Yin, A. M. Hong Cheung, K. S. Wong, S. K. So, H. Yan, A. Man, H. Cheung, K. S. Wong, S. Kong, C. Ma, J. Zhang, H. Yin, A. M. Hong Cheung, K. S. Wong, S. K. So, H. Yan, *Joule* **2020**, *4*, 1486.

[36] Y. Guo, W. Sato, K. Shoyama, H. Halim, Y. Itabashi, R. Shang, E. Nakamura, *J. Am. Chem. Soc.* **2017**, *139*, 9598.

[37] M. Li, C. Zhao, Z. Wang, C. Zhang, H. K. H. Lee, A. Pockett, J. Barbé, W. C. Tsoi, Y. Yang, M. J. Carnie, X. Gao, W. Yang, J. R. Durrant, L. Liao, S. M. Jain, *Adv. Energy Mater.* **2018**, *8*, 1801509.

[38] H. K. H. Lee, J. Barbé, S. M. P. Meroni, T. Du, C.-T. Lin, A. Pockett, J. Troughton, S. M. Jain, F. De Rossi, J. Baker, M. J. Carnie, M. A. McLachlan, T. M. Watson, J. R. Durrant, W. C. Tsoi, *Sol. RRL* **2019**, *3*, 1800207.

[39] R. Cheng, C. Chung, H. Zhang, F. Liu, W. Wang, Z. Zhou, S. Wang, A. B. Djurišić, S. Feng, *Adv. Energy Mater.* **2019**, *9*, 1901980.

[40] J. W. Lim, H. Kwon, S. H. Kim, Y.-J. You, J. S. Goo, D.-H. Ko, H. J. Lee, D. Kim, I. Chung, T. G. Kim, D. H. Kim, J. W. Shim, *Nano Energy* **2020**, *75*, 104984.

[41] H. Sun, K. Deng, Y. Jiang, J. Ni, J. Xiong, L. Li, *Small* **2020**, *16*, 1906681.

[42] M. Lee, E. Choi, A. M. Soufiani, J. Lim, M. Kim, D. Chen, M. A. Green, J. Seidel, S. Lim, J. Kim, X. Dai, R. Lee-Chin, B. Zheng, Z. Hameiri, J. Park, X. Hao, J. S. Yun, *Adv. Funct. Mater.* **2021**, *31*, 2008908.

[43] X. He, J. Chen, X. Ren, L. Zhang, Y. Liu, J. Feng, J. Fang, K. Zhao, S. (Frank) Liu, *Adv. Mater.* **2021**, *2100770*, 2100770.

[44] Y. C. Liu, H. H. Chou, F. Y. Ho, H. J. Wei, T. C. Wei, C. Y. Yeh, *J. Mater. Chem. A* **2016**, *4*, 11878.

[45] M. Freitag, J. Teuscher, Y. Saygili, X. Zhang, F. Giordano, P. Liska, J. Hua, S. M. Zakeeruddin, J.-E. Moser, M. Grätzel, A. Hagfeldt, *Nat. Photonics* **2017**, *11*, 372.

[46] Y. S. Tingare, N. S. Vinh, H.-H. Chou, Y.-C. Liu, Y.-S. Long, T.-C. Wu, T.-C. Wei, C.-Y. Yeh, *Adv. Energy Mater.* **2017**, *7*, 1700032.

[47] K. S. K. Reddy, Y. C. Liu, H. H. Chou, K. Kala, T. C. Wei, C. Y. Yeh, *ACS Appl. Mater. Interfaces* **2018**, *10*, 39970.

[48] M. L. Jiang, J. J. Wen, Z. M. Chen, W. H. Tsai, T. C. Lin, T. J. Chow, Y. J. Chang, *ChemSusChem* **2019**, *12*, 3654.

[49] R.-Y. Huang, W.-H. Tsai, J.-J. Wen, Y. J. Chang, T. J. Chow, *J. Power Sources* **2020**, *458*, 228063.

[50] E. Tanaka, H. Michaels, M. Freitag, N. Robertson, *J. Mater. Chem. A* **2020**, *8*, 1279.

[51] C. Y. Chen, Z. H. Jian, S. H. Huang, K. M. Lee, M. H. Kao, C. H. Shen, J. M. Shieh, C. L. Wang, C. W. Chang, B. Z. Lin, C. Y. Lin, T. K. Chang, Y. Chi, C. Y. Chi, W. T. Wang, Y. Tai, M. De Lu, Y. L. Tung, P. T. Chou, W. T. Wu, T. J. Chow, P. Chen, X. H. Luo, Y. L. Lee, C. C. Wu, C. M. Chen, C. Y. Yeh, M. S. Fan, J. De Peng, K. C. Ho, Y. N. Liu, H. Y. Lee, C. Y. Chen, H. W. Lin, C. Te Yen, Y. C. Huang, C. S. Tsao, Y. C. Ting, T. C. Wei, C. G. Wu, *J. Phys. Chem. Lett.* **2017**, *8*, 1824.

[52] A. Virtuani, E. Lotter, M. Powalla, *Sol. Energy Mater. Sol. Cells* **2006**, *90*, 2141.

[53] F. Chen, *Adv. Opt. Mater.* **2019**, *7*, 1800662.

[54] H. S. Ryu, S. Y. Park, T. H. Lee, J. Y. Kim, H. Y. Woo, *Nanoscale* **2020**, *12*, 5792.

[55] R. Steim, T. Ameri, P. Schilinsky, C. Waldauf, G. Dennler, M. Scharber, C. J. Brabec, *Sol. Energy Mater. Sol. Cells* **2011**, *95*, 3256.

[56] C. M. Proctor, T.-Q. Nguyen, *Appl. Phys. Lett.* **2015**, *106*, 083301.

[57] S. Zeiske, O. J. Sandberg, N. Zarrabi, W. Li, P. Meredith, A. Armin, *Nat. Commun.* **2021**, *12*, 3603.

[58] B. P. Lechêne, M. Cowell, A. Pierre, J. W. Evans, P. K. Wright, A. C. Arias, *Nano Energy* **2016**, *26*, 631.

[59] Y. Cui, L. Hong, J. Hou, *ACS Appl. Mater. Interfaces* **2020**, *12*, 38815.

[60] C. L. Cutting, M. Bag, D. Venkataraman, *J. Mater. Chem. C* **2016**, *4*, 10367.

[61] B. Minnaert, P. Veelaert, *Energies* **2014**, *7*, 1500.

[62] Y. Cui, L. Hong, T. Zhang, H. Meng, H. Yan, F. Gao, J. Hou, *Joule* **2021**, *5*, 1016.

[63] H. Yin, S. Chen, S. H. Cheung, H. W. Li, Y. Xie, S. W. Tsang, X. Zhu, S. K. So, *J. Mater. Chem. C* **2018**, *6*, 9111.

[64] Y. Cho, T. Kumari, S. Jeong, S. M. Lee, M. Jeong, B. Lee, J. Oh, Y. Zhang, B. Huang, L. Chen, C. Yang, *Nano Energy* **2020**, *75*, 104896.

[65] "Commission Internationale de l'Eclairage (CIE), CIE standard illuminant (CIE S 017:2020 ILV/17-23-021)," can be found under http://cie.co.at/eilvterm/17-23-021, **2020**.

[66] I. Fryc, P. Tabaka, *Opt. Appl.* **2019**, *49*, 345.

[67] H. Zheng, D. Li, C. Ran, Q. Zhong, L. Song, Y. Chen, P. Müller-Buschbaum, W. Huang, *Sol. RRL* **2021**, 2100042.

[68] M. Saliba, L. Etgar, *ACS Energy Lett.* **2020**, *5*, 2886.

[69] P. M. Sommeling, H. C. Rieffe, J. A. M. van Roosmalen, A. Schönecker, J. M. Kroon, J. A. Wienke, A. Hinsch, *Sol. Energy Mater. Sol. Cells* **2000**, *62*, 399.

[70] D. J. Wehenkel, K. H. Hendriks, M. M. Wienk, R. A. J. Janssen, *Org. Electron.* **2012**, *13*, 3284.

[71] P. Hartnagel, T. Kirchartz, *Adv. Theory Simulations* **2020**, *3*, 2000116.

[72] S. Beuel, P. Hartnagel, T. Kirchartz, *Adv. Theory Simulations* **2021**, *2000319*,

2000319.

[73] L. Hong, H. Yao, Z. Wu, Y. Cui, T. Zhang, Y. Xu, R. Yu, Q. Liao, B. Gao, K. Xian, H. Y. Woo, Z. Ge, J. Hou, *Adv. Mater.* **2019**, 1903441.

[74] W. Shockley, H. J. Queisser, *J. Appl. Phys.* **1961**, *32*, 510.

[75] P. W. Bridgman, *Phys. Rev.* **1928**, *31*, 101.

[76] M. F. Müller, M. Freunek, L. M. Reindl, *IEEE J. Photovoltaics* **2013**, *3*, 59.

[77] J. K. W. Ho, H. Yin, S. K. So, *J. Mater. Chem. A* **2020**, *8*, 1717.

[78] N. H. Reich, W. G. J. H. M. van Sark, E. A. Alsema, R. W. Lof, R. E. I. Schropp, W. C. Sinke, W. C. Turkenburg, *Sol. Energy Mater. Sol. Cells* **2009**, *93*, 1471.

[79] N. H. Reich, W. Van Sark, E. a Alsema, S. Y. Kan, S. Silvester, A. Van Der Heide, R. W. Lof, R. Schropp, *Proc 20th Eur. Photovolt. Sol. Energy ConfWIP* **2005**, 4.

[80] S. W. Glunz, J. Dicker, M. Esterle, M. Hermle, J. Isenberg, F. J. Kamerewerd, J. Knobloch, D. Kray, A. Leimenstoll, F. Lutz, D. Oßwald, R. Preu, S. Rein, E. Schäffer, C. Schetter, H. Schmidhuber, H. Schmidt, M. Steuder, C. Vorgrimler, G. Willeke, *Conf. Rec. IEEE Photovolt. Spec. Conf.* **2002**, 450.

[81] T. Kirchartz, P. Kaienburg, D. Baran, *J. Phys. Chem. C* **2018**, *122*, 5829.

[82] J. Yao, T. Kirchartz, M. S. Vezie, M. A. Faist, W. Gong, Z. He, H. Wu, J. Troughton, T. Watson, D. Bryant, J. Nelson, *Phys. Rev. Appl.* **2015**, *4*, 014020.

[83] T. Kirchartz, K. Taretto, U. Rau, *J. Phys. Chem. C* **2009**, *113*, 17958.

[84] J. Wong, S. T. Omelchenko, H. A. Atwater, *ACS Energy Lett.* **2021**, *6*, 52.

[85] L. J. A. Koster, S. E. Shaheen, J. C. Hummelen, *Adv. Energy Mater.* **2012**, *2*, 1246.

[86] M. Azzouzi, T. Kirchartz, J. Nelson, *Trends Chem.* **2019**, *1*, 49.

[87] S. Liu, J. Yuan, W. Deng, M. Luo, Y. Xie, Q. Liang, Y. Zou, Z. He, H. Wu, Y. Cao, *Nat. Photonics* **2020**, *14*, 300.

[88] X.-K. Chen, D. Qian, Y. Wang, T. Kirchartz, W. Tress, H. Yao, J. Yuan, M. Hülsbeck, M. Zhang, Y. Zou, Y. Sun, Y. Li, J. Hou, O. Inganäs, V. Coropceanu, J.-L. Bredas, F.

Gao, *Nat. Energy* **2021**, DOI 10.1038/s41560-021-00843-4.

[89] F. D. Eisner, M. Azzouzi, Z. Fei, X. Hou, T. D. Anthopoulos, T. J. S. Dennis, M. Heeney, J. Nelson, *J. Am. Chem. Soc.* **2019**, *141*, 6362.

[90] U. Rau, B. Blank, T. C. M. Müller, T. Kirchartz, *Phys. Rev. Appl.* **2017**, *7*, 044016.

[91] X. Hou, Y. Wang, H. K. H. Lee, R. Datt, N. Uslar Miano, D. Yan, M. Li, F. Zhu, B. Hou, W. C. Tsoi, Z. Li, *J. Mater. Chem. A* **2020**, *8*, 21503.

[92] N. An, Y. Cai, H. Wu, A. Tang, K. Zhang, X. Hao, Z. Ma, Q. Guo, H. S. Ryu, H. Y. Woo, Y. Sun, E. Zhou, *Adv. Mater.* **2020**, *32*, 2002122.

[93] W. Gao, H. Fu, Y. Li, F. Lin, R. Sun, Z. Wu, X. Wu, C. Zhong, J. Min, J. Luo, H. Y. Woo, Z. Zhu, A. K. Y. Jen, *Adv. Energy Mater.* **2021**, *11*, 2003177.

TOC Figure

D. Lübke, P. Hartnagel, J. Angona, T. Kirchartz

Comparing and Quantifying Indoor Performance of Organic Solar Cells

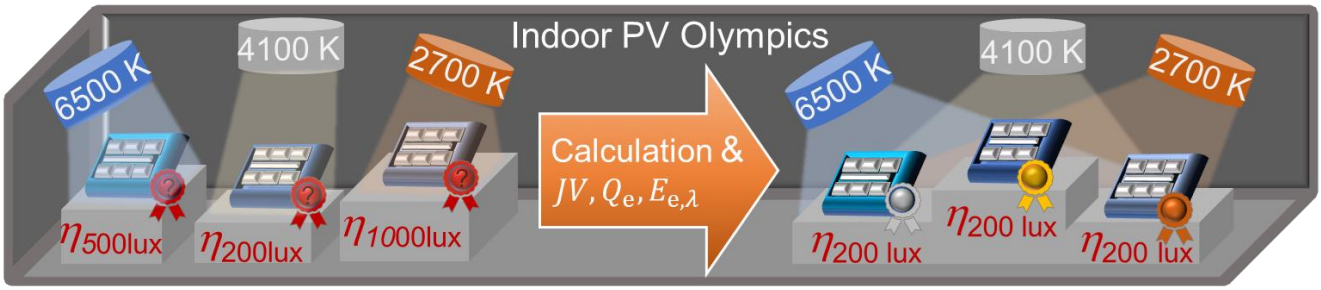

Although organic photovoltaics establish to be a promising candidate for indoor light recycling, there is a lack of standardized testing conditions to quantify the performance of solar cells. Therefore, we propose a method to calculate the efficiency of organic solar cells on the basis of relative emission spectra, *JV* and quantum efficiency measurements, which enables a fair ranking of champion solar cells.

Supporting Information

Comparing and Quantifying Indoor Performance of Organic Solar Cells

*Dana Lübke, Paula Hartnagel, Johanna Angona and Thomas Kirchartz**

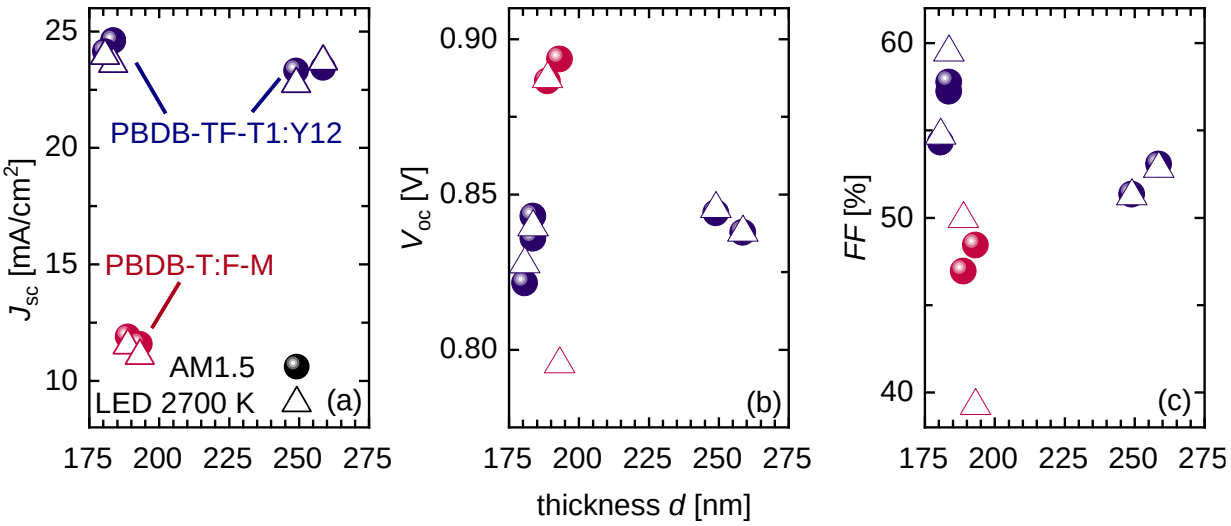

Figure S1. Comparison of J_{sc}, V_{oc} and FF values for an illumination under AM1.5 (triangles) and LED illumination with a color temperature of 2700 K (circles) of PBDB-T:F-M and PBDB-TF-T1:Y12 samples of different thicknesses. The overlap of the data for AM1.5 and LED illumination suggest that the resulting $V_{oc}(J_{sc})$ and $FF(J_{sc})$ points are independent of the used light source.

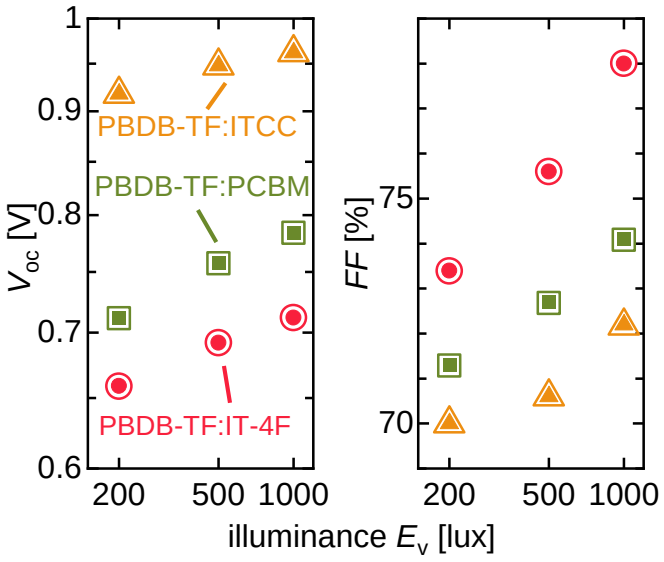

Figure S2. V_{oc} and FF values plotted against the illuminance on a double logarithmic scale using the data of Cui et al. [1] (filled symbols) and the data of our calculation (blank symbols).

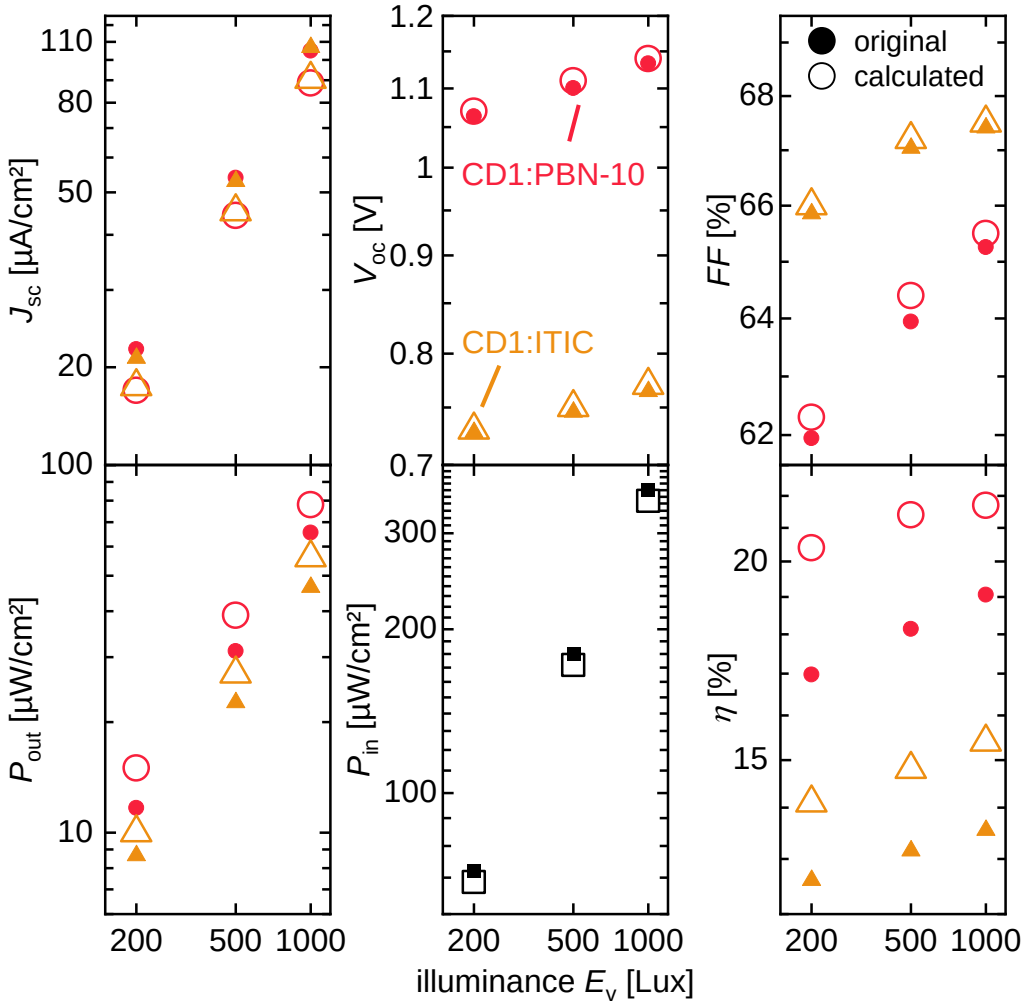

Figure S3. Comparison of original and calculated performance parameters and input powers of Ding et al.[2] Original values for the input power density result from the determination of the illuminance with a lux meter and relative spectral irradiance measurements, which is a highly uncertain method. Our calculation shows lower input powers P_{in} for all illuminances. For a set illuminance of 200 lux, the relative spectral irradiance is shifted by a factor f of 0.0104 and the calculated P_{in} should be 68.7 µW/cm². As the P_{in} in this publication is stated to be 72 µW/cm² (back calculated with the lux meter), the lux meter underestimates the irradiance by 5 % (theoretical $72\,\mu W/cm^2$ correlates to $200\,\text{lux} \cdot 72\,\mu W cm^{-2} / 68.7\,\mu W cm^{-2} \approx 210\,\text{lux}$). Therefore, the measured values of Ding et al. are mistakenly left-shifted on the x-axis and are located slightly to higher illumination levels in reality. As a consequence, the given $V_{oc}(J_{sc})$ and $FF(J_{sc})$ values are not measured at real 200 lux, but at a slightly higher illumination. As a result, the data of the theoretical calculation (with real 200 lux) give slightly lower J_{sc} and consequently V_{oc}, FF and P_{out} values.

As we now know, the given data for Ding et al. correlate to real 210 lux instead to the stated 200 lux, which is an error of 5 %. This error due to the wrongly determined P_{in} should

propagate linearly to the J_{sc}. For our calculation we find a J_{sc} of 18.1 µA/cm² for the CD1:ITIC sample. If the error due to P_{in} was the only error, Ding et al. should have measured $18.1\ \mu A/cm^2 \cdot 1.05 = 19\ \mu A/cm^2$, which is not the case as they state 21 µA/cm². Hence, apart from the discrepancy due to the undefined illumination level, there must be an additional discrepancy. We assume that the error is likely to be the discrepancy of theoretical J_{sc} values (from $Q_{e,PV}$ integration) and the J_{sc} values from *JV* measurements. As pointed out in Ref. [3], both J_{sc} values should be consistent to evaluate the device performance precisely.

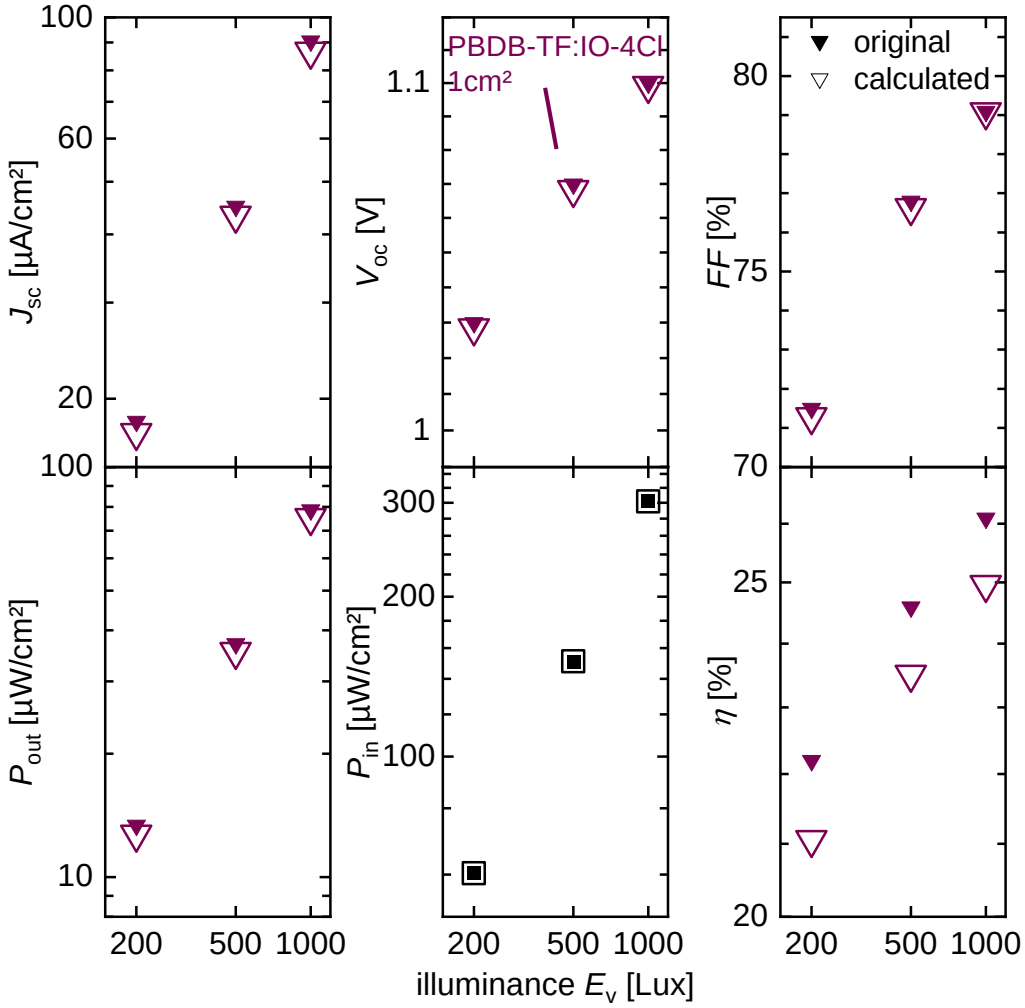

Figure S4. Stated performance parameters as in original reference (Cui et al., Nature Energy[4]) and from our calculations, which are in good accordance. We find a slight discrepancy in efficiency ~1 % as our calculated J_{sc} from $Q_{e,PV}$ is 17.3 µA/cm² and the reference gives the efficiencies with the J_{sc} from *JV* measurements.

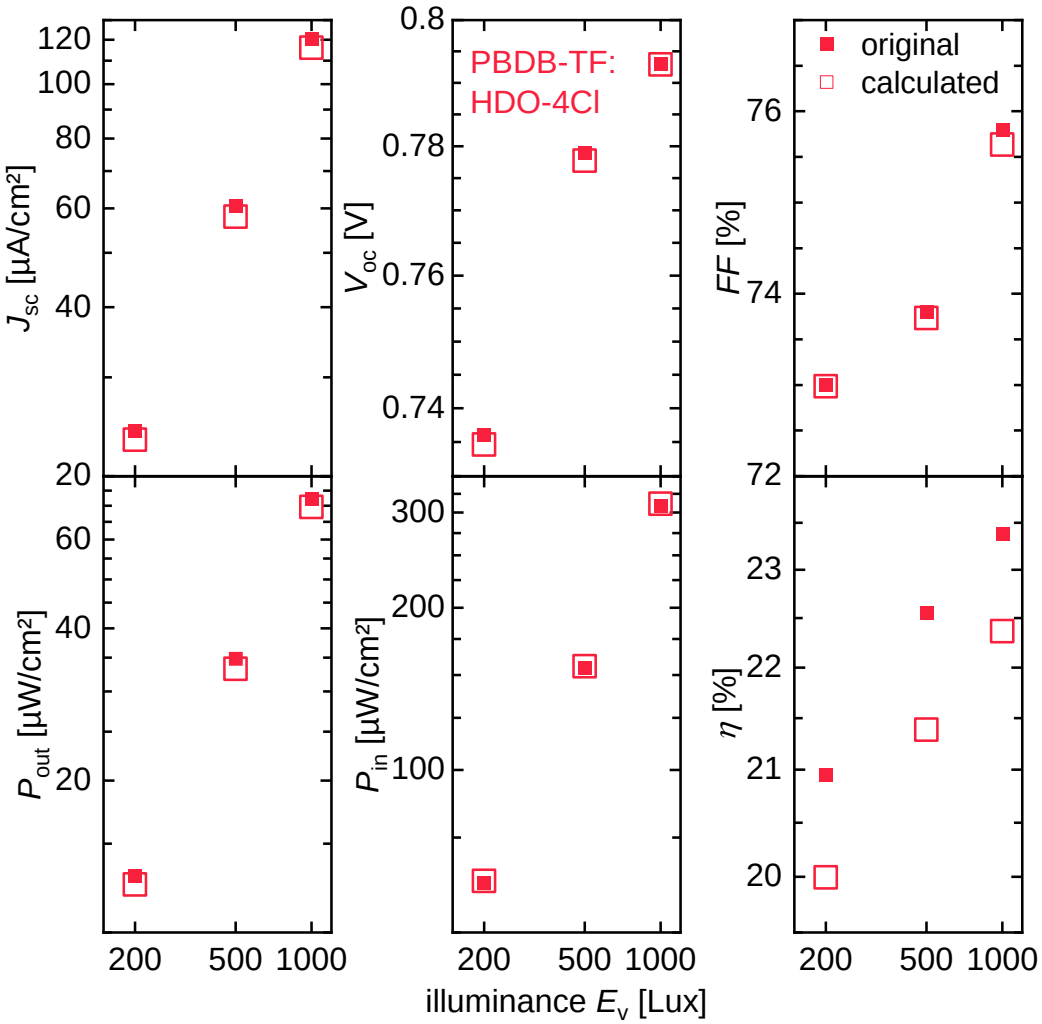

Figure S5. Stated performance parameters as in original reference (Xu et al.[5]) and from our calculations, which are in good accordance. Again, a slight discrepancy in efficiency ~1 % can be seen, as both methods use J_{sc} from different measurements (*JV* and $Q_{e,PV}$).

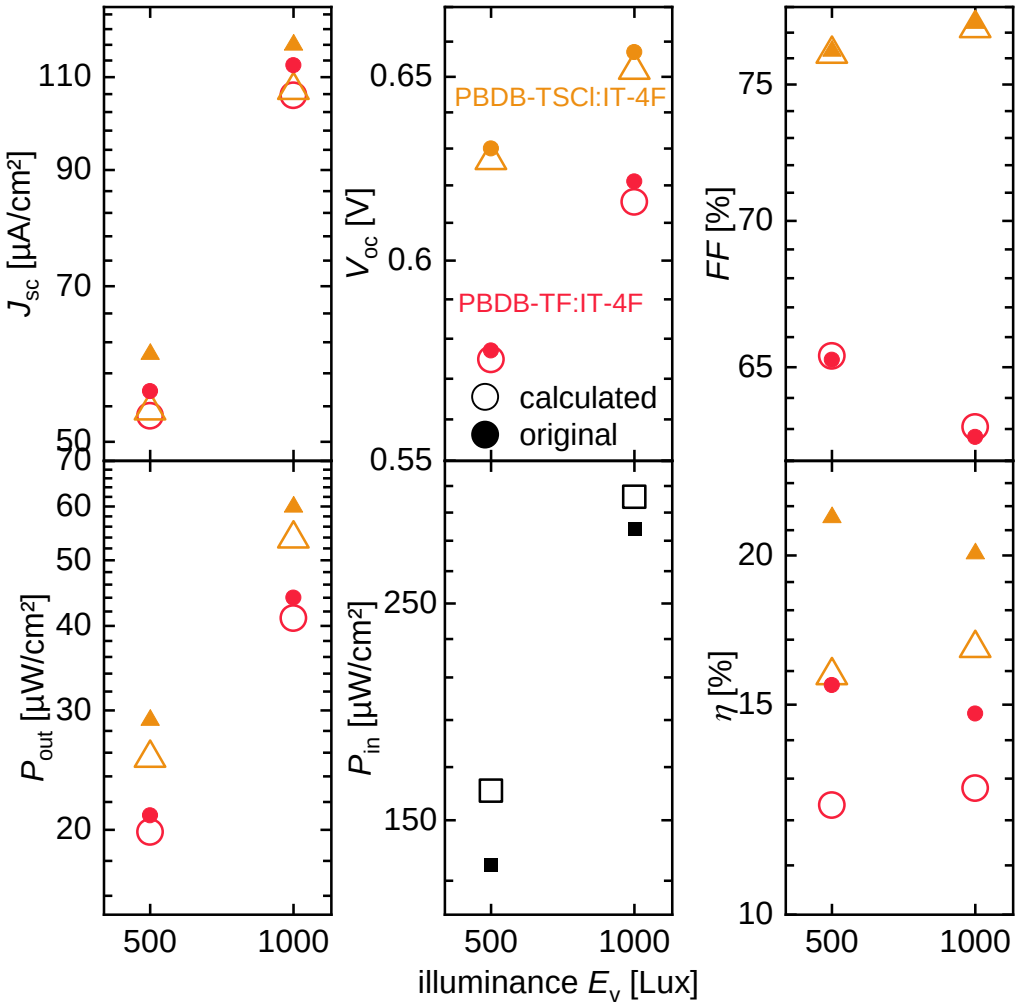

Figure S6. Stated performance parameters as in original reference (Park et al.[6]) and from our calculations. Wrongly determined P_{in} suggest an overestimation as the stated P_{in} from Park et al. (134.9 µA/cm²) would correlate to 416 lux instead of the given 500 lux. Therefore, lower J_{sc} compared to our calculated J_{sc} would be expected. As this is not the case, high differences in theoretical J_{sc} from $Q_{e,PV}$ and *JV* measurements are likely to be the reason for this discrepancy. In fact, J_{sc} from $Q_{e,PV}$ measurements for 1 sun illumination are ~2mA/cm² smaller compared to the J_{sc} from *JV* measurements, which is in accordance to the smaller calculated J_{sc} in Figure S7.

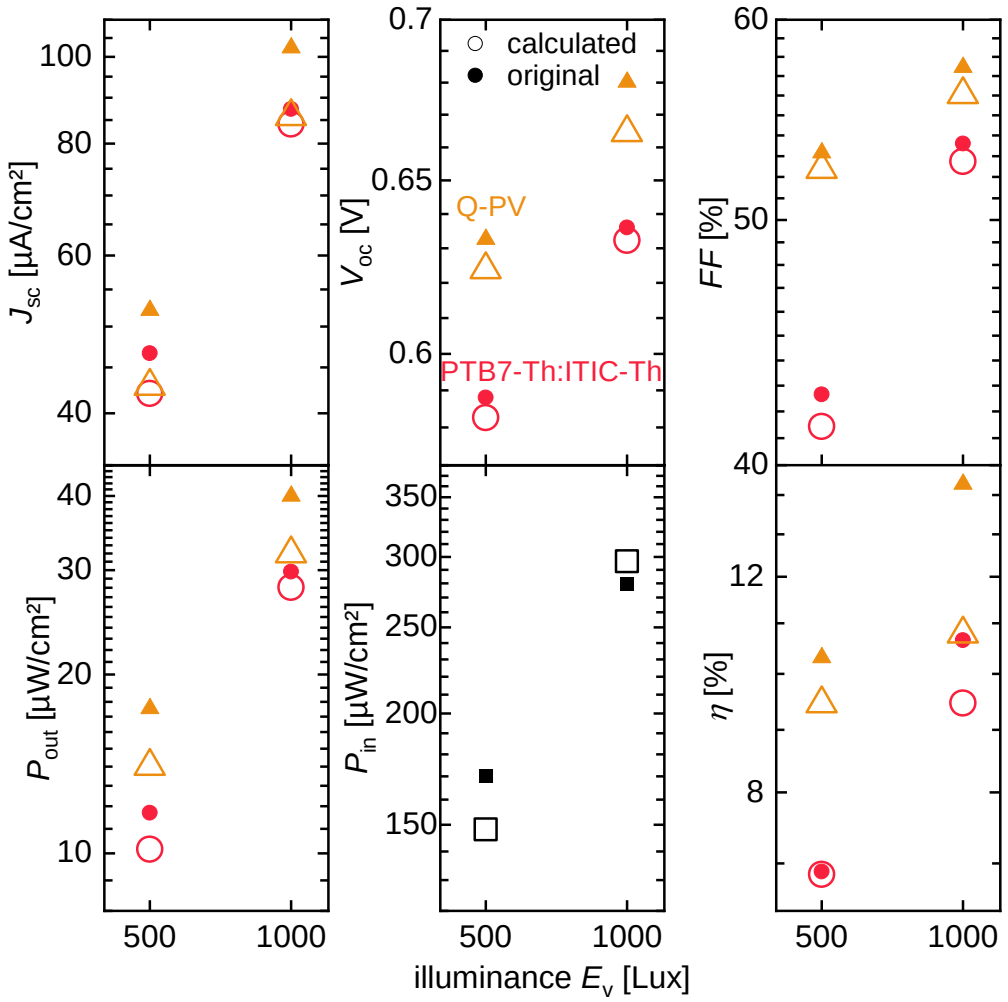

Figure S7. Stated performance parameters as in original reference (Nam et al.[7]) and from our calculations. Wrongly determined illuminance levels (e.g. stated 170 µW/cm² should refer to ~570 lux instead of the given 500 lux) and strong discrepancies in theoretical J_{sc} from $Q_{e,PV}$ and *JV* measurements lead to higher stated J_{sc} from the reference compared to the calculated ones.

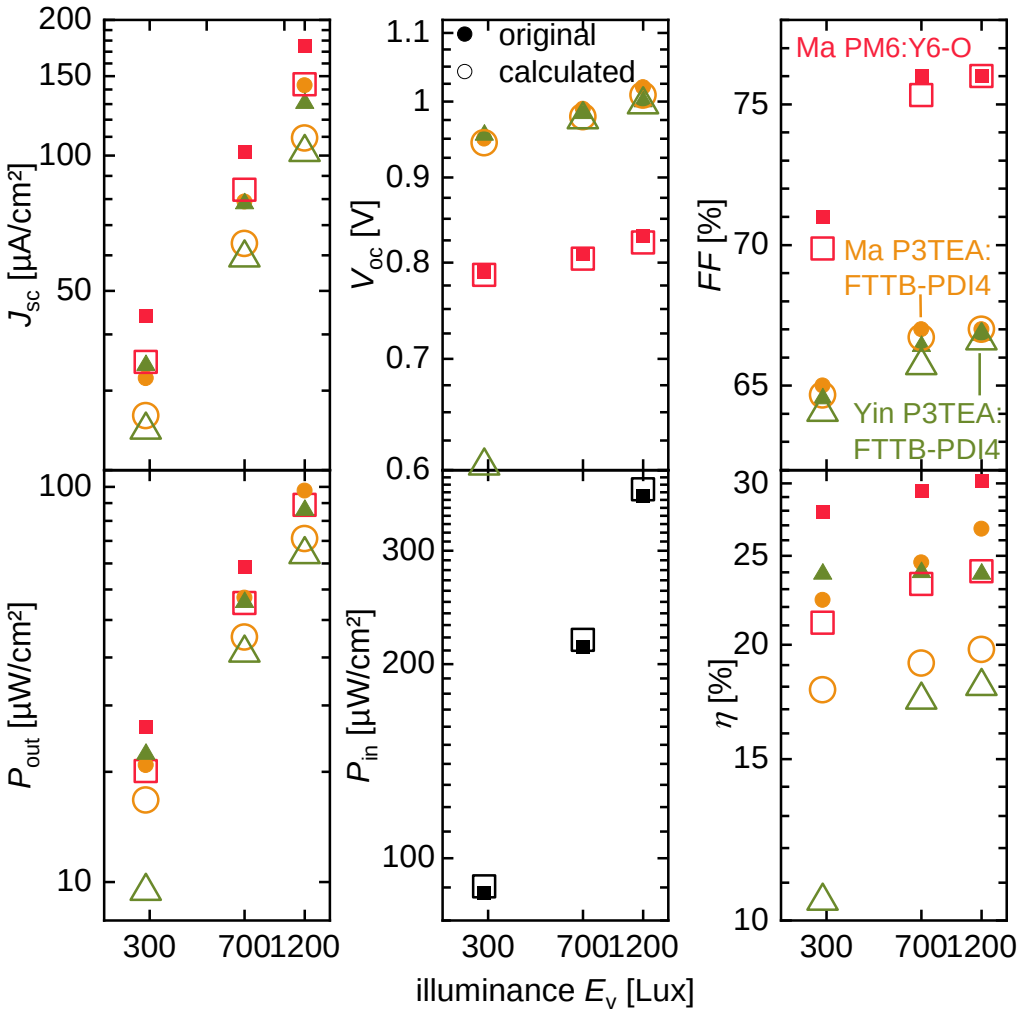

Figure S8. Stated performance parameters as in original reference (Ma et al.[8] and Yin et al.[9]) and from our calculations. For Ma et al. only the best cells with the electron transport layer PDI-NO and for Yin et al. the cells with the thickness of ~80 nm are considered. The J_{sc} data stated in the reference differ from our calculations significantly. We found 34.2 mA/cm², 26.4 mA/cm² and 24.5 mA/cm² for the PM6:Y6, P3TEA:FTTB-PDI4 of Ma et al. and the P3TEA:FTTB-PDI4 of Yin et al., respectively, opposed to the values in the reference of 44 mA/cm², 32 mA/cm², 34.2 mA/cm². These high differences cannot be the result due to the small discrepancy in P_{in}. In the reference of Ma et al. the calculated J_{sc} from $Q_{e,PV}$ are given and match well with the ones resulting from *JV* measurements, which is not the case for our data. As the $Q_{e,PV}$ data was reproduced with the software *Origin2020* one could assume wrongly reproduced data. In order to check whether our reproduced $Q_{e,PV}$ data is sufficiently correct, we calculated the J_{sc} from $Q_{e,PV}$ for AM1.5 irradiation. This amounts to 22.2 mA/cm² and 13.3 mA/cm² for the PM6:Y6-O and the P3TEA:FTTB-PDI4 sample of Ma et al., whereas the stated J_{sc} from $Q_{e,PV}$ in the reference was 22.53 mA/cm² and 13.52 mA/cm². Hence, the error due to the reproduced $Q_{e,PV}$ data is only in the region of ~2 %, which cannot explain the huge

differences in our calculated J_{sc}. To this point the discrepancy cannot be explained and should be further examined.

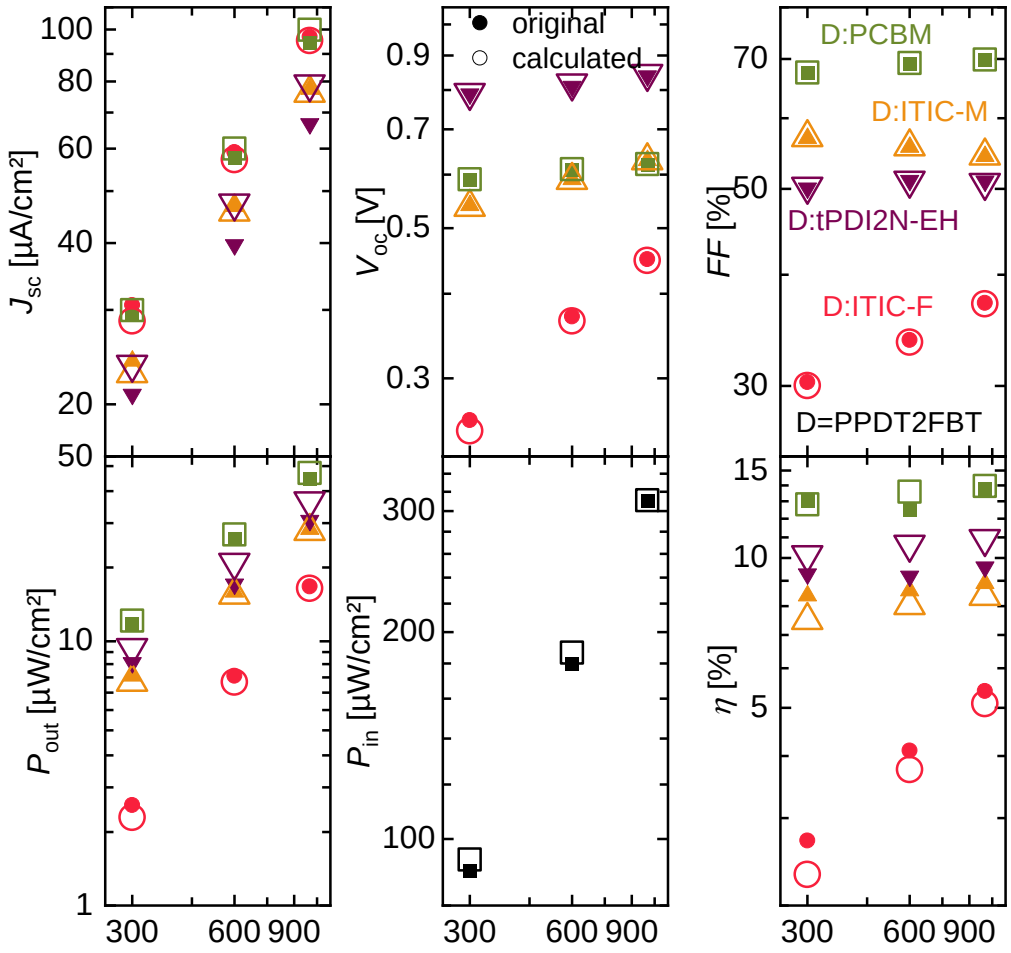

Figure S9. Stated performance parameters as in original reference (Dayneko et al.[10]) and from our calculations. Maximum J_{sc} deviation is found to be ~3µA/cm² and for the efficiency the maximum deviation is ~1%, suggesting measurements to be of sufficient quality.

Calculation of the Shockley-Queisser efficiency

The Shockley-Queisser (SQ) model uses the principle of detailed balance between absorption and emission and can be used to calculate the maximum efficiency of a solar cell.[11] Here, we show how to calculate the efficiency as in the original text, but with other artificial light sources. This calculation is similar to the calculations of Freunek et al. [12] and Ho et al.[13], but we use a set of LED lights sources with different spectra at constant illuminances and focus on the band gap dependence of the performance parameters. A detailed description of the efficiency calculation with the SQ model can also be found in Ref. [14].

The SQ model predicts that every photon with an energy above the energy gap E_g creates one electron hole-pair, which contributes to the short circuit current density

$$J_{sc,SQ} = q \int_{E_g}^{\infty} \varphi_{LED}\,(E)\mathrm{d}E, \tag{1}$$

where q is the elementary charge and φ_{LED} is the LEDs spectrum in units of $cm^{-2}s^{-1}eV^{-1}$. The principle of detailed balance[15] requires that an absorbing body also emits radiation, which is calculated by the excess luminescence flux $\Delta\Phi_{lum}$ from the solar cell[16]

$$\Delta\Phi_{lum} = \int_{E_g}^{\infty} \varphi_{bb}\,(E)\mathrm{d}E \left[\exp\left(\frac{qV}{kT}\right) - 1\right]. \tag{2}$$

Here, $V = \Delta E_f/q$ the internal voltage with the quasi-Fermi level splitting ΔE_f, φ_{bb} is the black body spectrum at the temperature T of the solar cell with h as Planck's constant, c as the speed of light and k as Boltzmann's constant:

$$\varphi_{bb}(E) = \frac{2\pi E^2}{h^3c^2}\frac{1}{[\exp(E/kT)-1]} \approx \frac{2\pi E^2}{h^3c^2}\exp\left(\frac{-E}{kT}\right). \tag{3}$$

As in the SQ limit radiative recombination is the only recombination possible, the current in the dark is the recombination current in the dark being $J_d = q\Delta\Phi_{lum}(V)$. This leading the pre-factor in Equation 2 to be interpreted as the saturation current density

$$J_{0,SQ} = q \int_{E_g}^{\infty} \varphi_{bb}\,(E, T = 300K)dE. \tag{4}$$

Consequently, the current-voltage curve under illumination in the SQ limit is

$$J = J_{0,SQ}\left[\exp\left(\frac{qV}{kT}\right) - 1\right] - J_{sc,SQ}, \tag{5}$$

which leads to the voltage at open-circuit $V_{oc,SQ}$

$$V_{\mathrm{oc,SQ}} = \frac{kT}{q} \ln\left(\frac{J_{\mathrm{sc,SQ}}}{J_{0,\mathrm{SQ}}} + 1\right). \quad (6)$$

To calculate the efficiency, the maximum of the extracted power density $P = -JV$ is divided by the incoming power density of the LED light source:

$$\eta_{SQ} = \frac{\max(P)}{\int_0^\infty E\varphi_{\mathrm{LED}}(E)\mathrm{d}E}. \quad (7)$$

The results of the efficiency calculation for a set of different light sources at a constant illuminance of 200 lux can found in Figure 3 in the main paper.

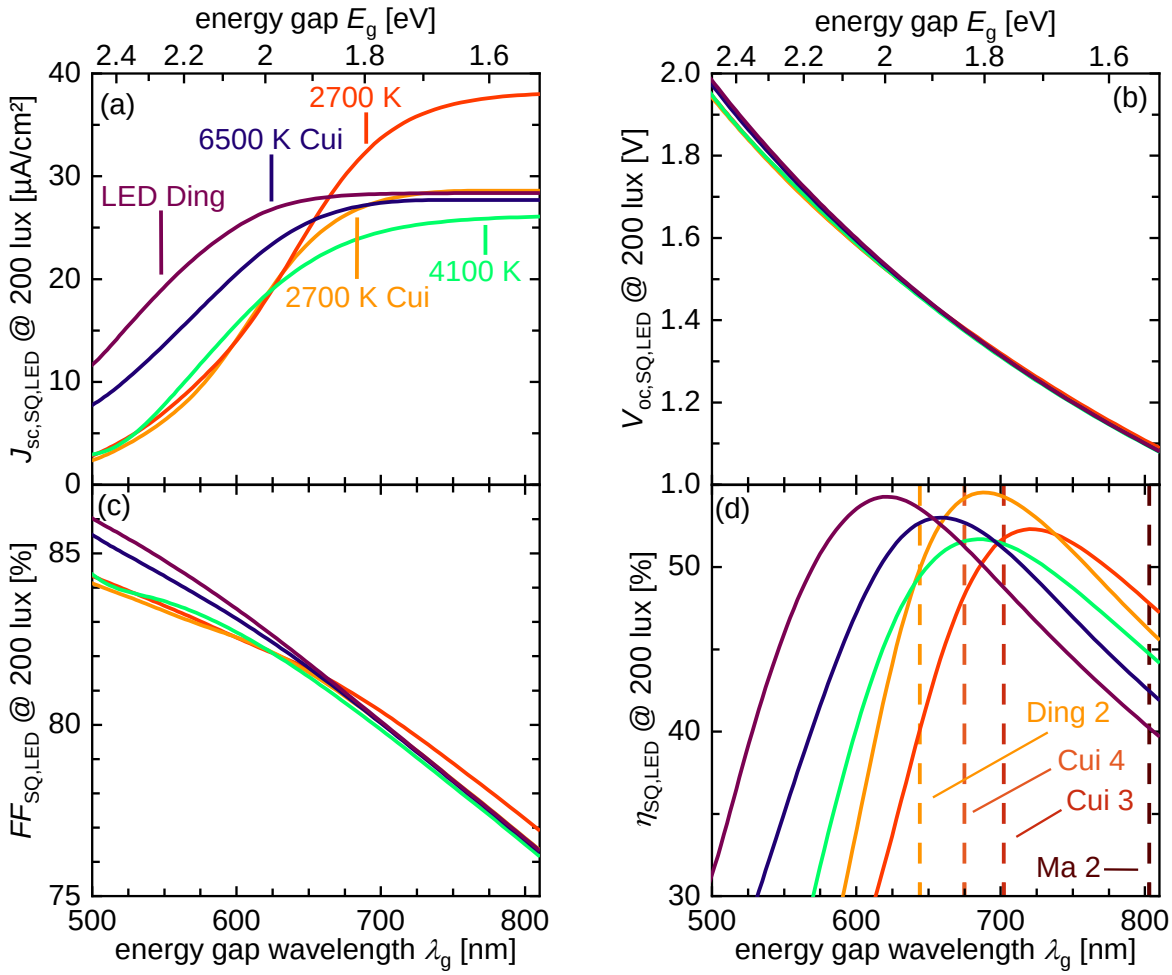

Figure S10. Performance parameters of the Shockley-Queisser model for a constant illuminance of 200 lux for different wavelengths λ_g of the energy gap. In the efficiency plot, vertical lines mark the energy gap wavelengths λ_g of some materials analyzed in section 3.2. Materials to the numbered code can be found in Table S1.

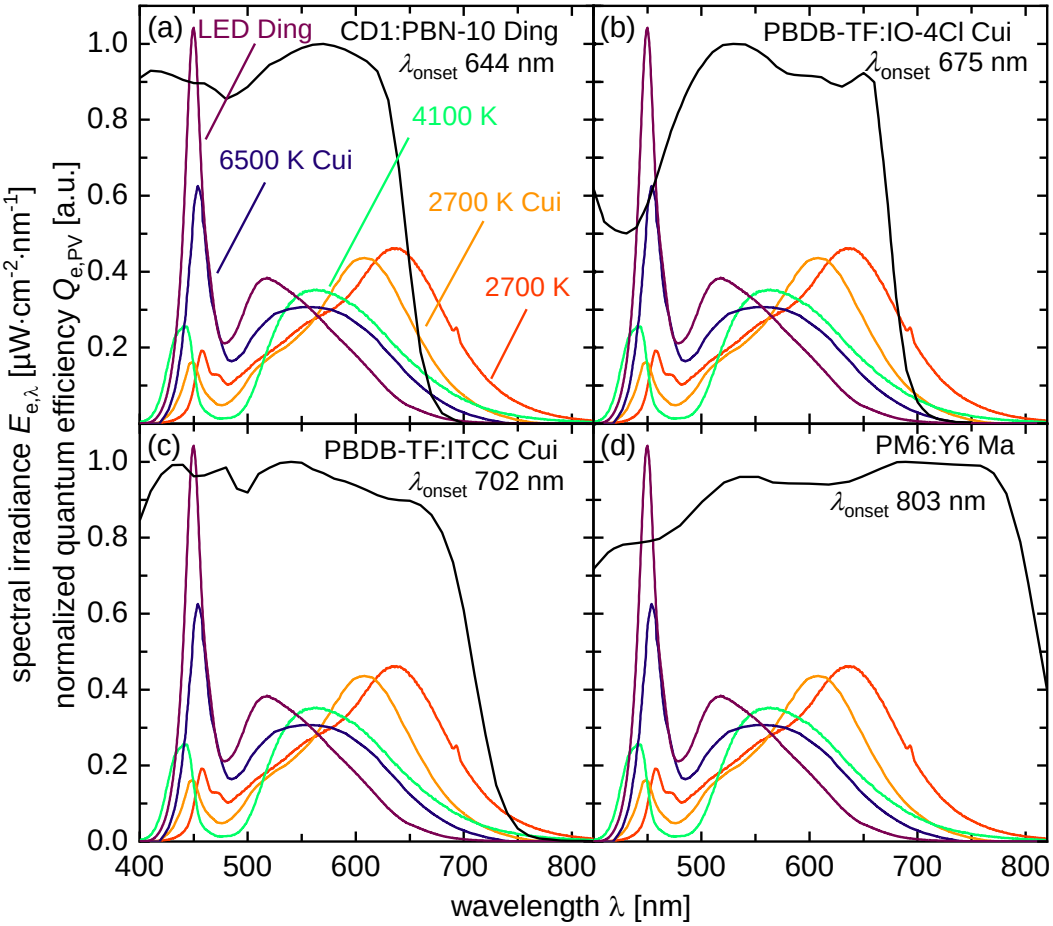

Figure S11. Normalized $Q_{e,PV}$ spectra of the analyzed samples in section 3.2 as well as spectral irradiances of the used light sources at 200 lux. The J_{sc} increases if the LED spectra shift toward a better absorbing region.

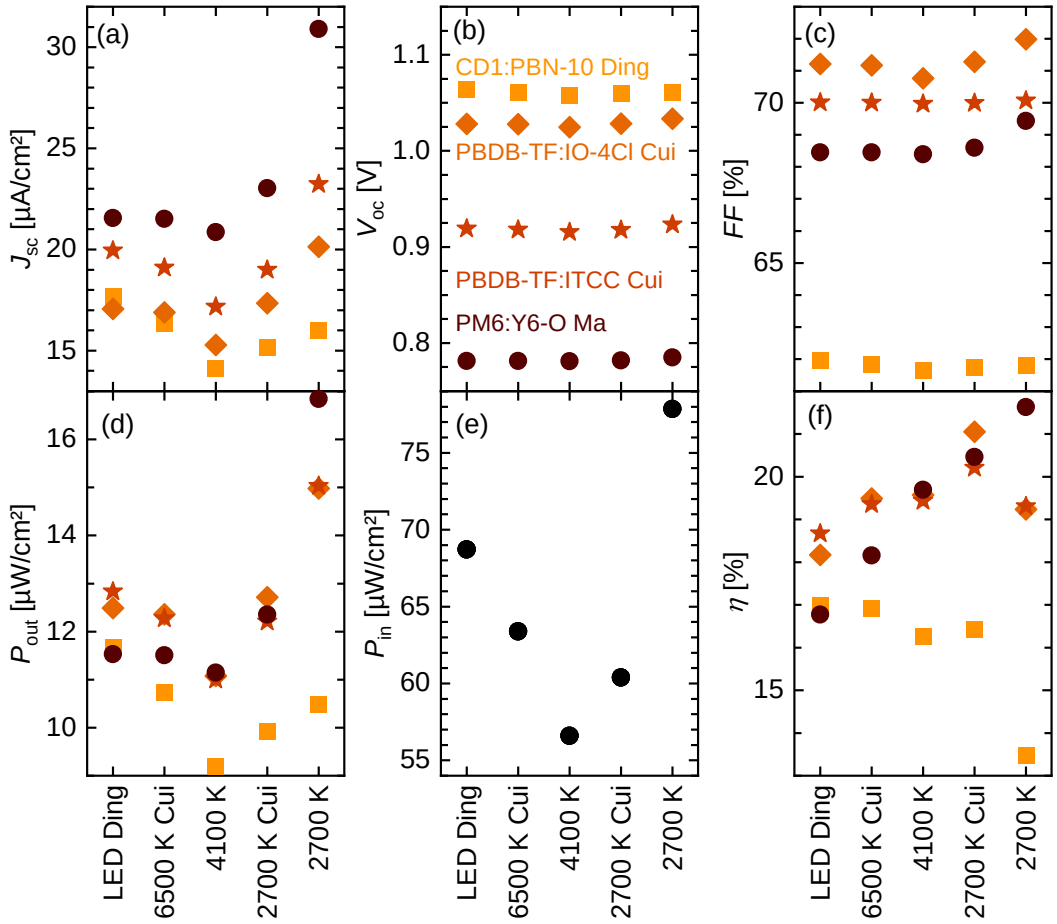

Figure S12. Absolute values of the performance parameters for different light sources, according to Figure 4 in the main paper.

Table S1. Performance parameters and wavelength of the energy gap λ_g for different publications at a constant illuminance of 200 lux sorted with increasing efficiencies. To rank the efficiencies, the calculation was done for the whole set of 5 LEDs, but only the highest resulting efficiency is shown. Input power densities for the LED of Ding et al., the LED with 2700 K of Cui et al. and the LED with 2700 K used in our group are 68.72 µW/cm², 60.38 µW/cm² and 77.85 µW/cm², respectively.

Abbr.	Ref.	Material	λ_g [nm]	LED	J_{sc} [µA/cm²]	V_{oc} [V]	*FF* [%]	P_{out} [µW/cm²]	η [%]
Dayn.	[10]	PPDT2FBT:ITIC-F	772	2700 K	25.8	0.25	29.8	1.9	2.4
Yin	[9]	P3TEA:FTTB-PDI4	716	2700 K	20.9	0.37	63.9	4.9	6.3
Nam	[7]	PTB7-Th:ITIC-Th	744	2700 K	25.2	0.57	36.5	5.3	6.8
Dayn.	[10]	PPDT2FBT:ITIC-M	744	2700 K	20.5	0.53	57.2	6.2	8.0
Dayn.	[10]	PPDT2FBT:tPDI2N-EH	679	2700 K Cui	15.8	0.78	49.7	6.1	10.2
Nam 1	[7]	Q-OPV	750	2700 K	26.3	0.62	54.2	8.9	11.4
Dayn.1	[10]	PPDT2FBT:$PC_{60}BM$	682	2700 K Cui	20.0	0.58	66.8	7.8	12.9
Lueb.1		PBDB-TF-T1:Y12	872	2700 K	28.8	0.60	57.9	10.1	12.9
Park 1	[6]	PBDB-TF:IT-4F	791	2700 K	28.4	0.56	66.5	10.5	13.5
Lueb.2		PBDB-T:F-M	713	2700 K Cui	18.7	0.72	60.7	8.1	13.5
Cui 1	[17]	PBDB-TF:$PC_{71}BM$	664	2700 K Cui	18.6	0.71	71.3	9.4	15.6
Ding 1	[2]	CD1:ITIC	750	2700 K	25.5	0.73	66.2	12.4	15.9
Je 1	[18]	PBDB-TS-4Cl:IT-4F	772	2700 K	27.8	0.63	73.7	12.9	16.6
Ding 2	[2]	CD1:PBN-10	644	LED Ding	17.7	1.06	61.9	11.7	17.0
Park 2	[6]	PBDB-TSCl:IT-4F	793	2700 K	28.7	0.62	75.7	13.4	17.2
Ma 1	[8]	P3TEA:FTTB-PDI4	723	2700 K Cui	17.8	0.94	64.2	10.7	17.7
Cui 2	[17]	PBDB-TF:IT-4F	792	2700 K	29.9	0.67	73.9	14.8	19.0
Cui 3	[17]	PBDB-TF:ITCC	702	2700 K Cui	19.0	0.92	70.0	12.2	20.2
Xu 1	[5]	PBDB-TF:HD-4Cl	812	2700 K	29.9	0.74	73.1	16.3	20.9
Cui 4	[1]	PBDB-TF:IO-4Cl 1cm²	675	2700 K Cui	17.3	1.03	71.3	12.7	21.1
Ma 2	[8]	PM6:Y6-O	803	2700 K	30.9	0.79	69.4	16.8	21.6

Table S2. Performance parameters and wavelength of the energy gap λ_g for different publications at a constant illuminance of 200 lux sorted with increasing λ_g. To rank the efficiencies, the calculation was done for the whole set of 5 LEDs, but only the highest resulting efficiency is shown Input powers for the LED of Ding et al., the LED with 2700 K of Cui et al. and the LED with 2700 K used in our group are 68.72 µW/cm², 60.38 µW/cm² and 77.85 µW/cm², respectively.

Abbr.	Ref.	Material	λ_g [nm]	LED	J_{sc} [µA/cm²]	V_{oc} [V]	*FF* [%]	P_{out} [µW/cm²]	η [%]
Ding 2	[2]	CD1:PBN-10	644	LED Ding	17.7	1.06	61.9	11.7	17.0
Cui 1	[17]	PBDB-TF:$PC_{71}BM$	664	2700 K Cui	18.6	0.71	71.3	9.4	15.6
Cui 4	[1]	PBDB-TF:IO-4Cl 1cm²	675	2700 K Cui	17.3	1.03	71.3	12.7	21.1
Dayn.	[10]	PPDT2FBT:tPDI2N-EH	679	2700 K Cui	15.8	0.78	49.7	6.1	10.2
Dayn.1	[10]	PPDT2FBT:$PC_{60}BM$	682	2700 K Cui	20.0	0.58	66.8	7.8	12.9
Cui 3	[17]	PBDB-TF:ITCC	702	2700 K Cui	19.0	0.92	70.0	12.2	20.2
Lueb.2		PBDB-T:F-M	713	2700 K Cui	18.7	0.72	60.7	8.1	13.5
Yin	[9]	P3TEA:FTTB-PDI4	716	2700 K	20.9	0.37	63.9	4.9	6.3
Ma 1	[8]	P3TEA:FTTB-PDI4	723	2700 K Cui	17.8	0.94	64.2	10.7	17.7
Nam	[7]	PTB7-Th:ITIC-Th	744	2700 K	25.2	0.57	36.5	5.3	6.8
Dayn.	[10]	PPDT2FBT:ITIC-M	744	2700 K	20.5	0.53	57.2	6.2	8.0
Nam 1	[7]	Q-OPV	750	2700 K	26.3	0.62	54.2	8.9	11.4
Ding 1	[2]	CD1:ITIC	750	2700 K	25.5	0.73	66.2	12.4	15.9
Dayn.	[10]	PPDT2FBT:ITIC-F	772	2700 K	25.8	0.25	29.8	1.9	2.4
Je 1	[18]	PBDB-TS-4Cl:IT-4F	772	2700 K	27.8	0.63	73.7	12.9	16.6
Park 1	[6]	PBDB-TF:IT-4F	791	2700 K	28.4	0.56	66.5	10.5	13.5
Cui 2	[17]	PBDB-TF:IT-4F	792	2700 K	29.9	0.67	73.9	14.8	19.0
Park 2	[6]	PBDB-TSCl:IT-4F	793	2700 K	28.7	0.62	75.7	13.4	17.2
Ma 2	[8]	PM6:Y6-O	803	2700 K	30.9	0.79	69.4	16.8	21.6
Xu 1	[5]	PBDB-TF:HD-4Cl	812	2700 K	29.9	0.74	73.1	16.3	20.9
Lueb.1		PBDB-TF-T1:Y12	872	2700 K	28.8	0.60	57.9	10.1	12.9

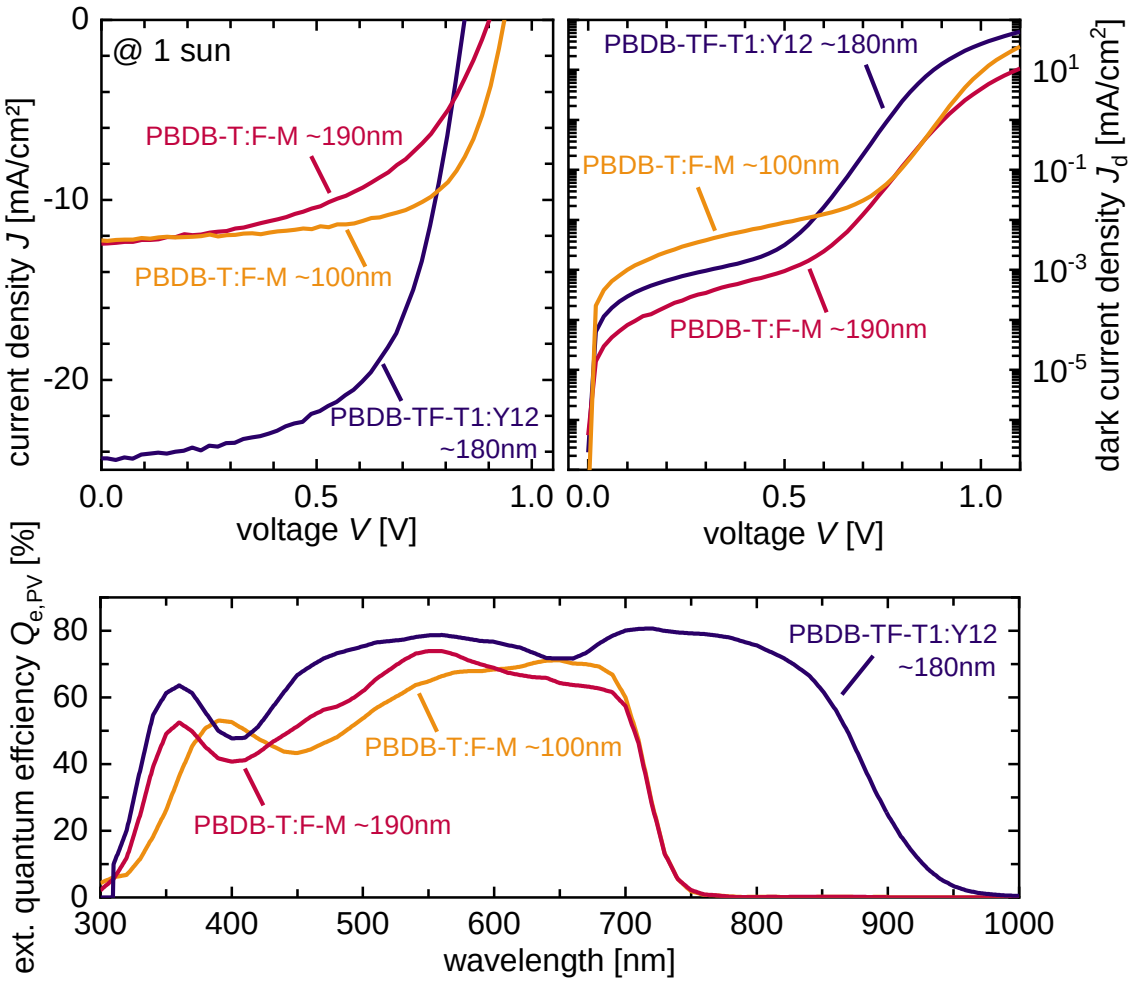

Figure S13. *JV* measurements under 1 sun illumination (corrected as stated in the method section) and in the dark and external quantum efficiency measurements of PBDB-T:F-M and PBDB-TF-T1:Y12 devices fabricated in our group. Listed parameters can be found in Table S3.

Table S3. Device performance of OPV devices fabricated for this work under 1 sun illumination.

Material	thickness d[a] [nm]	active area A [cm²]	J_{sc} [mA/cm²]	$J_{sc,cal}$[b] [mA/cm²]	V_{oc} [V]	FF [%]	η [%]	$\eta_{,cal}$[b] [%]
PBDB-T:F-M	100	0.16	12.3	13.1	0.93	65.1	7.4	8.0
PBDB-T:F-M	190	0.16	12.4	13.5	0.89	49.9	5.5	6.0
PBDB-T:F-M	240	0.06	12.8		0.94	43.6	5.7	
PBDB-TF-T1:Y12	180	0.16	24.4	24.0	0.84	59.5	12.2	12.0

[a)] estimated with capacitance-voltage measurements [b)] calculated from $Q_{e,PV}$ measurements.

Table S4. Device performance of OPV devices under illumination with a 2700 K LED for the interpolation of $V_{oc}(J_{sc})$ and $FF(J_{sc})$ pairs according to the presented method. The illuminance was estimated with a lux meter.

Material	Illuminance[a] [lux]	J_{sc} [μA/cm²]	V_{oc} [V]	FF [%]	P_{out} [μW/cm²]	Filter OD
PBDB-T:F-M (~240 nm, 0.06 cm²)	200.5	37.5	0.73	61.0	16.8	1.5
	310.6	58.2	0.75	61.8	27.0	1.5
	470.5	88.5	0.77	63.3	43.2	1.5
	724	136.1	0.79	63.5	68.1	1.5
	1082	198.3	0.80	64.4	102.5	1.5
PBDB-T:F-M (~190 nm, 0.16 cm²)	203.7	41.2	0.73	62.6	18.9	2.0
PBDB-T1-TF:Y12 (~180 nm, 0.16 cm²)	46.2	20.1	0.58	55.0	6.5	2.0
	85.6	33.3	0.61	58.7	11.9	2.0
	203.7	73.4	0.64	62.9	29.7	2.0
	436	151.3	0.67	65.8	67.0	2.0
	940	310.4	0.70	67.3	146.7	2.0

[a] illuminance estimated with a lux meter.

References

[1] Y. Cui, Y. Wang, J. Bergqvist, H. Yao, Y. Xu, B. Gao, C. Yang, S. Zhang, O. Inganäs, F. Gao, J. Hou, *Nat. Energy* **2019**, *4*, 768.

[2] Z. Ding, R. Zhao, Y. Yu, J. Liu, *J. Mater. Chem. A* **2019**, *7*, 26533.

[3] Y. Cui, L. Hong, J. Hou, *ACS Appl. Mater. Interfaces* **2020**, *12*, 38815.

[4] Y. Cui, Y. Wang, J. Bergqvist, H. Yao, Y. Xu, B. Gao, C. Yang, S. Zhang, O. Inganäs, F. Gao, J. Hou, *Nat. Energy* **2019**, *4*, 768.

[5] Y. Xu, H. Yao, L. Ma, Z. Wu, Y. Cui, L. Hong, Y. Zu, J. Wang, H. Y. Woo, J. Hou, *Mater. Chem. Front.* **2021**, *5*, 893.

[6] S. Park, H. Ahn, J. J. Y. J. J. Y. J. Kim, J. B. Park, J. J. Y. J. J. Y. J. Kim, S. H. Im, H. J. Son, *ACS Energy Lett.* **2020**, *5*, 170.

[7] M. Nam, H. Y. Noh, J. Cho, Y. Park, S. C. Shin, J. J. A. J. J. A. Kim, J. J. A. J. J. A. Kim, H. H. Lee, J. W. Shim, D. H. Ko, *Adv. Funct. Mater.* **2019**, *29*, 1.

[8] L. K. Ma, Y. Chen, P. C. Y. Y. Chow, G. Zhang, J. Huang, C. Ma, J. Zhang, H. Yin, A. M. Hong Cheung, K. S. Wong, S. K. So, H. Yan, A. Man, H. Cheung, K. S. Wong, S. Kong, C. Ma, J. Zhang, H. Yin, A. M. Hong Cheung, K. S. Wong, S. K. So, H. Yan, *Joule* **2020**, *4*, 1486.

[9] H. Yin, L. Ma, J. Yan, Z. Zhang, A. M. H. Cheung, J. Zhang, H. Yan, S. K. So, *Sol.*

RRL **2020**, *4*, 2000291.

[10] S. V. Dayneko, M. Pahlevani, G. C. Welch, *ACS Appl. Mater. Interfaces* **2019**, 1.

[11] W. Shockley, H. J. Queisser, *J. Appl. Phys.* **1961**, *32*, 510.

[12] M. F. Müller, M. Freunek, L. M. Reindl, *IEEE J. Photovoltaics* **2013**, *3*, 59.

[13] J. K. W. Ho, H. Yin, S. K. So, *J. Mater. Chem. A* **2020**, *8*, 1717.

[14] T. Kirchartz, U. Rau, *Adv. Energy Mater.* **2018**, *8*, 1703385.

[15] P. W. Bridgman, *Phys. Rev.* **1928**, *31*, 101.

[16] P. Wurfel, *The Chemical Potential of Radiation*, **1982**.

[17] Y. Cui, H. Yao, T. Zhang, L. Hong, B. Gao, K. Xian, J. Qin, J. Hou, *Adv. Mater.* **2019**, *31*, 1904512.

[18] H. Il Je, E. Y. Shin, K. J. Lee, H. Ahn, S. Park, S. H. Im, Y. H. Kim, H. J. Son, S. K. Kwon, *ACS Appl. Mater. Interfaces* **2020**, *12*, 23181.